

Accounts

Control of the Magnetic and Optical Properties in Molecular Compounds by Electrochemical, Photochemical and Chemical Methods

Osamu Sato,* Shinya Hayami,† Yasuaki Einaga,†† Zhong-Ze Gu

Special Research Laboratory for Optical Science, Kanagawa Academy of Science and Technology, KSP Bldg. East 412, 3-2-1 Sakado, Takatsu-ku, Kawasaki 213-0012

†Department of Chemistry, Faculty of Science, Kyushu University, 6-10-1 Hakozaki, Higashi-ku, Fukuoka 812-8581

††Department of Applied Chemistry, Keio University, 3-14-1 Hiyoshi, Kohoku-ku, Yokohama 223-8522

(Received May 20, 2002)

The electrochemical, photochemical and chemical control of the magnetic properties in molecular compounds is described. The preparation of various thin films of CrCr and FeFe Prussian blue on a conducting electrode allowed us to control the magnetic properties by varying the oxidation state of the component metals. The magnetic properties of CrCr Prussian blue show that the critical temperature and coercive field can be drastically modified by electrochemical treatment. That is, the compound, $Cr^{II}_{1.29}Cr^{III}_{0.14}[Cr^{III}(CN)_6]$ has ferrimagnetic properties with T_c (critical temperature) = 240 K and H_c (coercive field) = 25 G, while the reduced form, $KCr^{II}_{1.29}Cr^{III}_{0.14}[Cr^{II}(CN)_6]$, has T_c = 100 K and H_c = 220 G. Similarly, it was found that the critical temperature of FeFe Prussian blue shifts continuously from paramagnetic to magnetic with T_c = 12 K. These changes can be expressed as $K_4Fe^{II}_4[Fe^{II}(CN)_6]_3$ (paramagnetic) $\leftrightarrows$ $Fe^{III}_4[Fe^{II}(CN)_6]_3$ (ferromagnetic, T_c = 4.5 K) + 4 K^+ + 4e^- and $Fe^{III}_4[Fe^{II}(CN)_6]_3$ (ferromagnetic, T_c = 4.2 K) + 3Cl^- − 3e^- $\leftrightarrows$ $Fe^{III}_4[Fe^{III}(CN)_6]_3(Cl)_3$ (T_c = 12 K). Furthermore, we have discovered that the FeCo Prussian blue and Co valence tautomeric compounds exhibit photo-reversible magnetization effects. The photoinduced magnetization in FeCo Prussian blue is expressed as $Na_{0.4}Co^{II\text{-}HS}{}_{0.3}Co^{III\text{-}LS}[Fe^{II}(CN)_6]$ (paramagnetic) $\leftrightarrows$ $Na_{0.4}Co^{II\text{-}HS}{}_{1.3}[Fe^{III}(CN)_6]$ (ferrimagnetic, T_c = 26 K and H_c = 6000 G), where HS and LS denote high-spin and low-spin. An example of the photoinduced valence tautomeric behavior is expressed as $[Co^{III\text{-}LS}$(3,5-dbsq)(3,5-dbcat)(tmeda)] $\leftrightarrows$ $[Co^{II\text{-}HS}$(3,5-dbsq)$_2$(tmeda)], where tmeda, 3,5-dbsq and 3,5-dbcat represent *N*,*N*,*N*′,*N*′-tetramethylethylenediamine, 3,5-di-*tert*-butyl-1,2-semiquinonate and 3,5-di-*tert*-butyl-1,2-catecholate, respectively. Additionally, we succeeded in tuning the phase transition temperature by varying the ligand field of the Co ions in the FeCo Prussian blue. Brief comments are also included regarding the first examples of light-induced excited spin state trapping observed in an Fe^{III} complex, i.e. $[Fe^{III\text{-}LS}(pap)_2]ClO_4\cdot H_2O$ $\leftrightarrows$ $[Fe^{III\text{-}HS}(pap)_2]$-$ClO_4\cdot H_2O$ (pap = N-2-pyridylmethylidene-2-hydroxy-phenylaminato) and a photoinduced structural change observed in a Cu^{II} complex, $[Cu^{II}(dieten)_2](BF_4)_2$ [dieten = bis(*N*,*N* -diethylethylenediamine)].

There has been a great interest in developing novel molecule-based inorganic solids whose physical properties can be controlled by external perturbation.[1–3] Recently, we have been focusing our attention on the electrochemical, photochemical and chemical tuning of physical properties in the molecular compounds.[4–29] A key to the achievement of electrochemical control of the physical properties is the preparation of electroactive molecular compounds on conducting electrodes in the form of a thin film. In fact, the electrochromic properties of electrodeposited thin films have been extensively investigated.[2] On the other hand, we recently proposed the new concept of "Electrochemical Magnetization" and indeed succeeded in demonstrating a first example of the electrochemical tuning of magnetic properties using the electro-active property of Prussian blue analogues (Fig. 1).[4] This topic is described in Section 1.

Furthermore, together with the electrochemical magnetization, we have started a new project, i.e. the development of a molecule-based photo-magnet. Research into the interdisciplinary field between the magnetic and optical properties is one of the most attractive subjects because of its more fundamental aspects as well as its practical applications. Through the exploration of a large number of inorganic solids we have discovered that variants of FeCo Prussian blue, such as $Na_{0.4}Co_{1.3}$-$[Fe(CN)_6]$, exhibit photo-induced magnetization effects. This finding opens a new field of "Photoswitchable Magnets".[6,7,9] This topic, as well as the chemical tuning of the phase transition temperature in FeCo Prussian blue is described in Section 2.

In section 3 and 4, we describe three examples of optically

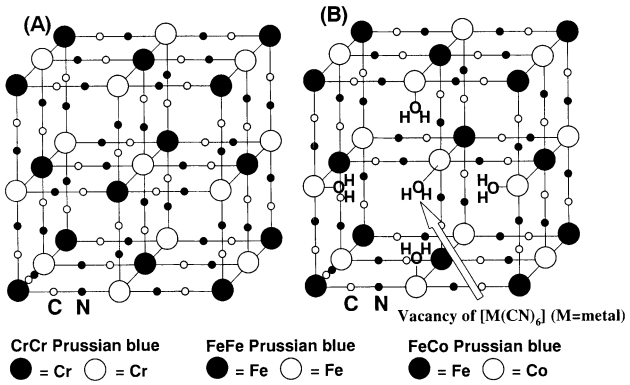

Fig. 1. (A) Structure of Prussian blue analogues with no defects. (B) Structure of Prussian blue analogues with $[M(CN)_6]$ vacancies. It is thought that the vacancies at the $[M(CN)_6]$ site are surrounded by six water molecules. Interstitial alkali cations are omitted for clarity.

switchable molecular solids. It is important to note that, until now, the number of optically switchable molecular solids available has been quite small. This is because, in order to achieve optical switching in molecular solids, conflicting requirements have to be satisfied simultaneously. On the one hand, the structural change accompanying the switching phenomena should not be too large, because steric effects often prevent the photochemical transformation. For example, the azobenzene derivatives, which are representative photochromic molecules, never show a trans-to-cis photo-isomerization due to steric hindrance in the solid state. On the other hand, the structural change should not be too small, because the relaxation probability from metastable states to stable states by tunneling increases with decreasing structural change. Such an example was seen in Fe^{III} spin crossover complexes. The photo-induced Fe^{III} high-spin states rapidly revert to the original low-spin states by tunneling effects at low temperature.[3,30] Hence, even if the compounds have nearly degenerate electronic states, most of them never exhibit photo-induced switching with long-lived metastable states. In order to prevent the rapid relaxation from a metastable state to the ground state, we recently proposed the introduction of strong inter-molecular interactions in molecular compounds.[25] The cooperativity resulting from the molecular interaction operates to increase the activation energy for the relaxation processes, enabling the observation of a long-lived metastable state after illumination. That is, when the metastable molecular orientation reverts to the stable orientation, a large stress field might be built up in such compounds because of the presence of a strong binding energy between molecules. Hence, even if the structural change is small, it is probable that the relaxation caused by tunneling effects can be substantially prevented. Based on this strategy, we have attempted to produce optically switchable coordination compounds, and have actually succeeded in observing these switching effects in several compounds. These include cobalt valence tautomeric compounds,[20–24] an Fe^{III} spin-crossover complex[25] and a Cu^{II} thermochromic complex,[26] in which ligand-to-ligand interlocking, π–π interaction and hydrogen bonding respectively play key roles. In the present paper, the photo-magnetic properties of the Co valence tautomeric compounds are described in detail in Section 3. Furthermore, brief descriptions of an Fe^{III} spin-crossover complex and a Cu^{II} thermochromic complex are given in Section 4. Finally, we introduce a recent advancement in the development of photo-magnetic materials in Section 5, and we then summarize our work in the last section.

1. Electrochemical Control of Magnetic Properties in Prussian Blue Analogues[4,5]

The magnetic properties of molecular compounds including Prussian blue analogues (Fig. 1) have recently attracted great attention.[31–37] One of the important challenges in this field is the development of a high T_c compound.[38–41] In 1999, the high T_c compounds $KV^{II}[Cr^{III}(CN)_6]$, for which T_c = 376 K,[42] and $K_{0.058}V^{II/III}[Cr^{III}(CN)_6](SO_4)_{0.058}\cdot 0.93H_2O$, for which T_c = 375 K,[43] were reported. In contrast, we are now focusing on the Prussian blue analogues from the viewpoint of the electrochemical control of their magnetic properties as well as the preparation of high T_c compounds.[4] Electrochemical reduction can be applied to the synthesis of Prussian blue analogues in the form of thin films (Fig. 2),[2,44] which provides a way of controlling the structure of the thin films by means of the electrode potential and thereby potentially raising T_c. Furthermore, the oxidation state of the metal ions constituting the films can be electrochemically controlled by making use of their electroactive properties and their thin film form, allowing modification of their magnetic properties after preparation. Based on this idea, we have fabricated electrochemically tunable molecule-based magnets, i.e. CrCr Prussian blue and FeFe Prussian blue.[4,5] Note that CrCr Prussian blue and FeFe Prussian blue represent the Prussian blue analogues with Cr-CN-Cr and Fe-CN-Fe moieties, respectively.

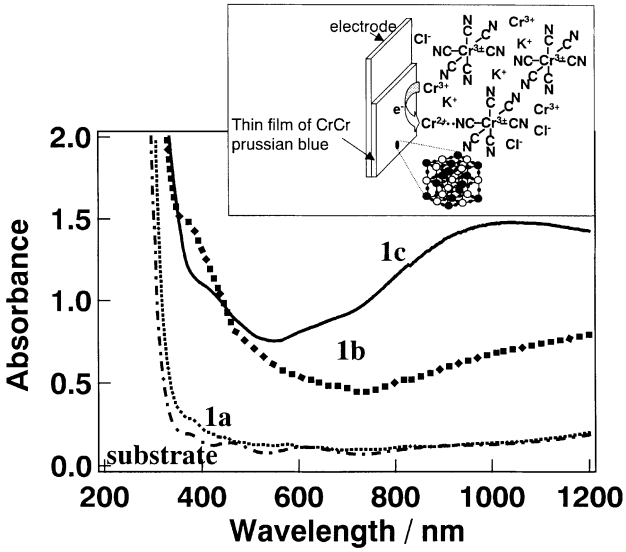

Fig. 2. Absorption spectra of **1a**, **1b** and **1c**. Inset: Electrochemical reduction technique for the preparation of the CrCr Prussian blue analogues. The compounds were prepared under the potentiostatic mode. The electrode potential was kept at −840 mV vs SCE (**1a**), −760 mV vs SCE (**1b**) and −760 mV vs SCE in the presence of 1 M CsCl (**1c**).[4]

1-1. Electrochemical Preparation of Transparent CrCr Prussian Blue Analogues. Mixed valence chromium polycyanides were synthesized via the electrochemical route. Previously, they were synthesized as fine powders by means of the reaction of substitution-inert $K_3[Cr^{III}(CN)_6]$ with labile Cr^{II}.[39] In the electrochemical technique, a labile chemical species is generated by electrochemical reduction in an aqueous solution of the substitution inert $K_3[Cr^{III}(CN)_6]$ and $Cr^{III}Cl_3 \cdot 6H_2O$.[4,5,45,46]

The procedure for the electrochemical route is as follows. Aqueous solutions containing 40 mM $Cr^{III}Cl_3 \cdot 6H_2O$ and 40 mM $K_3[Cr^{III}(CN)_6]$ were prepared separately. The solutions were then mixed and electrochemical reduction was performed using a Pt working electrode or a transparent conducting electrode in the mixed solution. The electrode potential was maintained at -840 mV or -760 mV vs a saturated calomel reference electrode (SCE). It has been reported that the redox potential of $[Cr^{III}(CN)_6]^{3-}$ is -1.38 V vs SCE.[47] Hence, the ideal electrochemical process is expressed as

$$Cr^{III}(\text{substitution inert}) + e^- \rightarrow Cr^{II}(\text{substitution labile})$$
$$[Cr^{III}(CN)_6]^{3-} + 1.5Cr^{II} \rightarrow Cr^{II}{}_{1.5}[Cr^{III}(CN)_6]$$

That is, the Cr^{III} moieties were changed to labile Cr^{II} moieties by the electrochemical reduction route on a working electrode. The generation of the labile species results in the formation of the Cr^{III}-CN-Cr^{II} structure via the coordination reaction of the labile Cr^{II} moieties with the $[Cr^{III}(CN)_6]^{3-}$ ions.

An important characteristic of the CrCr Prussian blue analogues is that the composition of these magnetic materials strongly depends on the electrochemical preparation conditions. Here we describe the magnetic properties of three typical materials, i.e. $Cr_{1.43}[Cr(CN)_6] \cdot 6.09H_2O$ (**1a**), $Cr_{1.12}[Cr(CN)_6] \cdot 2.80H_2O$ (**1b**) and $Cs_{1.15}Cr_{1.06}[Cr(CN)_6] \cdot 1.78H_2O$ (**1c**). Their UV-vis absorption spectra are shown in Fig. 2. It should be emphasized that **1a** is a colorless magnetic thin film, which is distinguishable from the classical opaque magnets. The successful preparation of such a transparent molecular magnetic film, as opposed to the powder form, allows us to regulate the polarization of light due to magneto-optical effects. Recently, Ohkoshi et al. and Ikeda et al. have reported magneto-optical properties and magnetization-induced second harmonic generation in thin films of the Prussian blue analogues for the first time, which is an important development in the field of molecular magnets.[48,49]

Buser et al. have carried out a single crystal analysis of Prussian blue, $Fe^{III}{}_4[Fe^{II}(CN)_6]_3 \cdot 15H_2O$, which suggests that Prussian blue has a face centered cubic (fcc) structure.[50] The powder X-ray diffraction patterns of the present compounds are consistent with the fcc structure. Their unit cell parameters were 10.41, 10.44 and 10.39 Å for **1a**, **1b** and **1c**, respectively.

1-2. Magnetic Properties of CrCr Prussian Blue Analogues. Firstly, let us briefly mention the magnetic coupling of the component metals in the Prussian blue analogues.[51,52] In order to understand the magnetic coupling, we should recall a super-exchange mechanism through the CN ligands, i.e. the kinetic exchange mechanism and the potential exchange mechanism.[53–56] It has been reported that the kinetic exchange mechanism plays a key role when the magnetic orbitals overlap each other. In this case, an antiferromagnetic interaction operates because of the Pauli principle. On the other hand, a potential exchange mechanism also plays a key role when magnetic orbitals with comparable orbital energies are orthogonal to each other. In this case, Hund's rule leads to a parallel spin alignment, i.e. a ferromagnetic interaction.

In the case of the present compounds, the exchange interactions can be divided into two types by neglecting the interaction between the next-nearest neighbors. The t_{2g} orbital of Cr^{III} or $Cr^{II\text{-}LS}$ at the carbon ends and the e_g orbital of the $Cr^{II\text{-}HS}$ at the nitrogen ends are orthogonal to each other. In this situation, the potential exchange mechanism becomes dominant, leading to a ferromagnetic interaction. The other interaction between the t_{2g} orbital of Cr^{III} or $Cr^{II\text{-}LS}$ at the carbon ends and the t_{2g} orbital of the $Cr^{II\text{-}HS}$ or Cr^{III} at the nitrogen ends, which overlap each other, gives rise to an antiferromagnetic character. When the ferromagnetic and antiferromagnetic interactions are superimposed, the antiferromagnetic term in general dominates the interactions. Therefore, ferrimagnetic properties are expected for the present compounds.

The magnetic properties are shown in Figs. 3, 4 and 5. The

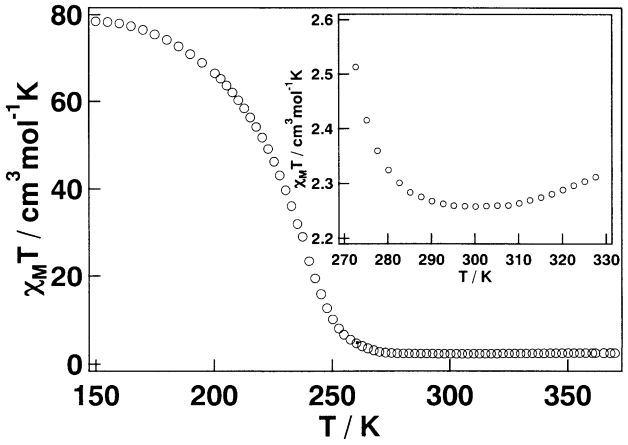

Fig. 3. $\chi_M T$ versus T plot of **1a**. Inset: Expanded plot from 270 to 330 K.[4]

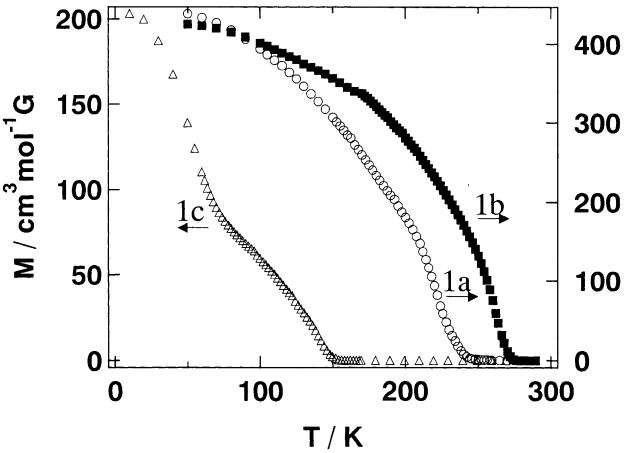

Fig. 4. Temperature dependence of the magnetization of compounds **1a** (○), **1b** (■) and **1c** (△).[4]

Table 1. Magnetic Properties of **1a**–**1c** before and after Eelectrochemical Reduction. Red **1a**, **1b** and **1c** Denote the Reduced Form of **1a**, **1b** and **1c**, Respectively. Hysteresis (M_r and H_c) and Magnetization (M) at 5 T Are Measured at 5 K

	1a	Red of **1a**	**1b**	Red of **1b**	**1c**	Red of **1c**
T_c/K	240	100	270	150	150	100
M_r/cm^3 mol^{-1} G	1204	—	1130	—	1290	—
H_c/G	25	220	143	370	130	530
C/cm^3 mol^{-1} K	4.58	—	4.14	—	4.03	—
θ/K	−320	—	−416	—	−119	—
M at 5 T/μ_B	0.7	—	0.5	—	0.7	—

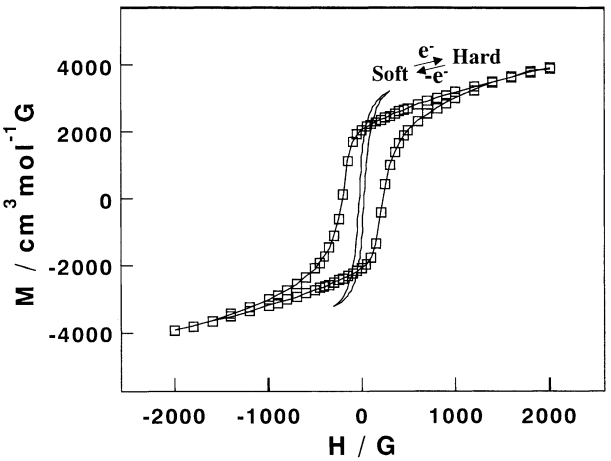

Fig. 5. Hysteresis loops of compounds **1a** before and after electrochemical reduction.

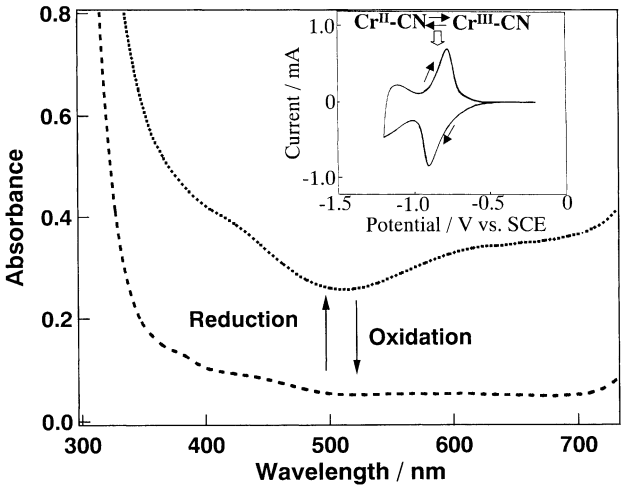

Fig. 6. UV-vis absorption spectra before and after electrochemical reduction of **1a**. Inset: Cyclic voltammogram of compound **1a**.[5]

product of the molar magnetic susceptibility and temperature, $\chi_M T$, versus temperature plot for compound **1a** first decreased upon cooling and then increased at lower temperatures (Fig. 3), indicating a short range antiferromagnetic interaction between the paramagnetic centers bearing different numbers of unpaired electrons (ferrimagnetism). This is consistent with the expected interaction described above. The Curie constant (C) and the Weiss constant (θ) are 4.58 cm^3 mol^{-1} K and −320 K, respectively. The field-cooled magnetization (FCM) versus temperature plots at H (magnetic field) = 0.5 mT (T = tesla) displayed an abrupt break at T_c = 240 K (Fig. 4). The field dependence of the magnetization (5 K) yielded a magnetization at H = 5 T of about 0.7 μ_B per **1a**. The magnetic hysteresis loop at 5 K yielded a remnant magnetization (M_r) of 1204 cm^3 mol^{-1} G and a coercive field (H_c) of 25 G (Fig. 5). Similar ferrimagnetic behavior is observed for compounds **1b** and **1c** (Table 1). The FCM vs T plots of **1b** and **1c** are shown in Fig. 4.

1-3. Electrochemical Control of Magnetic Properties in CrCr Prussian Blue. The electrochemical properties were investigated in 1 M KCl solutions. The prepared magnetic films were used as a working electrode. Pt and SCE were used as the counter and reference electrodes, respectively. Figure 6 shows the cyclic voltammogram of **1a**. The magnetic films were biased from −1.2 to −0.2 V vs SCE. The redox reactions proceeded reversibly and were accompanied by a color change (Fig. 6). Voltammometric peaks were observed at around −0.84 V vs SCE. The changes in the IR spectra show that the peak at 2187 cm^{-1} decreased after electrochemical reduction and a new peak appeared at 2071 cm^{-1}. They are ascribable to the CN stretching peaks in the Cr^{III}-CN-Cr^{II} structure and the Cr^{II}-CN-Cr^{II} structure, respectively. The UV-vis spectra shows a color change from colorless to bluish green. The change in the electronic structure can be expressed by

$$Cr^{II}_{1.29}Cr^{III}_{0.14}[Cr^{III}(CN)_6] + K^+ + e^- \rightarrow KCr^{II}_{1.29}Cr^{III}_{0.14}[Cr^{II}(CN)_6]$$

Furthermore, a small redox peak is observed at −1.2 V vs SCE. This indicates the presence of Cr^{III} moieties at the nitrogen ends, which undergo a redox reaction. Similar reversible redox reactions were observed for **1b** and **1c**.

The changes in the magnetic properties are shown in Fig. 7 and in Table 1. The FCM curve after reduction at −0.84 V shows an abrupt break at 100 K. This means that the critical temperature can be controlled by the electrochemical route. In the temperature region between 100 K and 240 K, the magnetic properties can be switched between ferrimagnetic and paramagnetic and vice versa via an electrochemical route. Similarly, after the electrochemical redox reaction, the critical temperatures for **1b** and **1c** change between 270 K and 150 K and between 150 K and 100 K, respectively.

The hysteresis loop of **1a** after reduction at −0.84 V yielded H_c = 220 G at 5 K (Fig. 5). This means that the coercive field could also be controlled between 25 G and 220 G by the electrochemical method. Hence, when the reduced form of **1a** un-

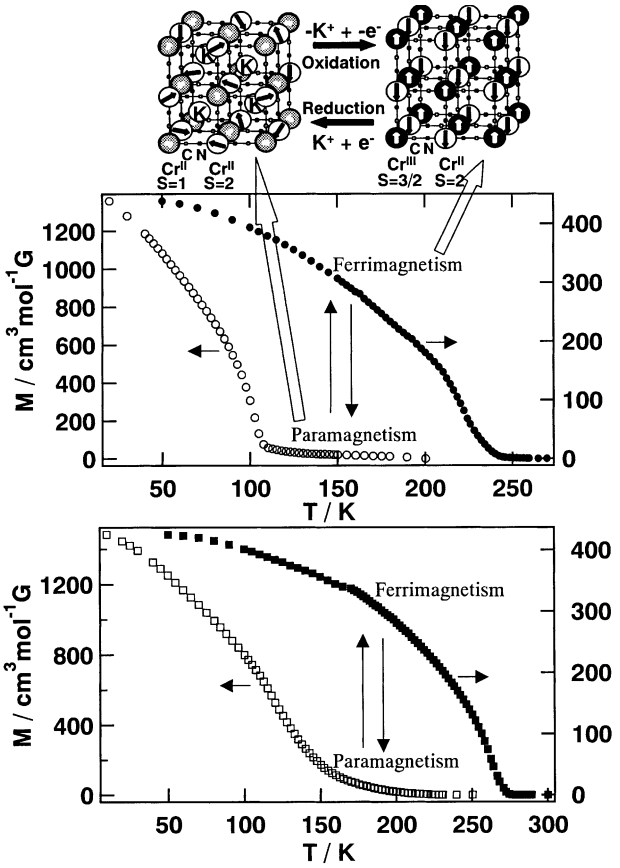

Fig. 7. Temperature dependence of the magnetization of compounds **1a** (top) and **1b** (bottom) before and after electrochemical reduction, and schematic illustration of the electrochemical control of the magnetic properties in CrCr Prussian blue.[4]

der an external magnetic field of between 25 G and 220 G is subjected to electrochemical oxidation followed by reduction, the direction of the magnetic polarity can be inverted. This provides a novel route for recording information in magnetic recording media.

1-4 Electrochemical Control of Magnetic Properties in FeFe Prussian Blue. Electrochemical control is also applicable to other Prussian blue analogues.[2,57–59] Here we describe another typical example of the changes in magnetic properties observed for FeFe Prussian blue (**1d**). The Prussian blue film was synthesized via the electrochemical route in a galvanostatic mode (ca. 25 mA/cm^2) onto conducting transparent electrodes.[44] The X-ray diffraction pattern was consistent with an fcc structure. The lattice parameter was 10.13 Å. When the magnetic films were biased from −0.3 to 1.2 V vs SCE, the redox reactions proceeded reversibly and were accompanied by a color change. Voltammometric peaks were observed at around 0.2 and 0.9 V vs SCE (Fig. 8). The electrochemical reduction process at 0.2 V can be expressed by

$$Fe^{III}_4[Fe^{II}(CN)_6]_3 \text{ (Prussian blue)} + 4K^+ + 4e^- \rightarrow K_4Fe^{II}_4[Fe^{II}(CN)_6]_3.$$

On the other hand, the electrochemical oxidation process at 0.9

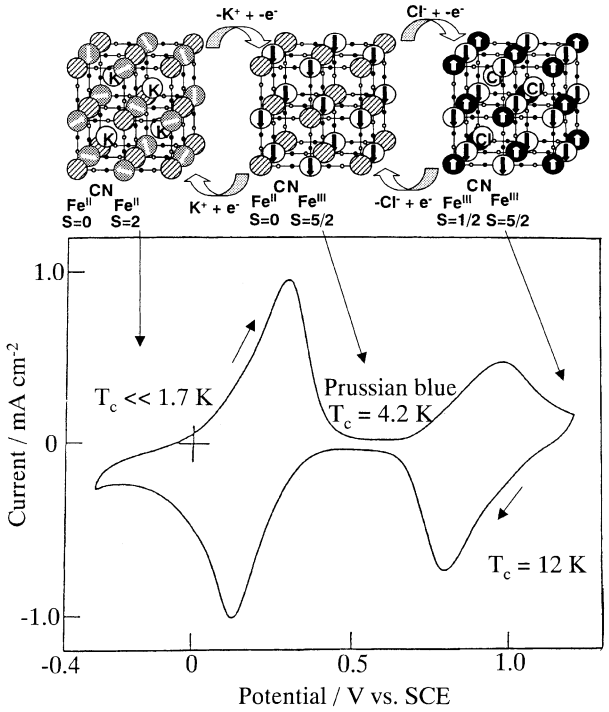

Fig. 8. Cyclic voltammogram of compound **1d**, and schematic illustration of the electrochemical control of the magnetic properties in FeFe Prussian blue.

V can be expressed by

$$Fe^{III}_4[Fe^{II}(CN)_6]_3 \text{ (Prussian blue)} + 3Cl^- - 3e^- \rightarrow Fe^{III}_4[Fe^{III}(CN)_6]_3(Cl)_3.$$

The change in the critical temperature is shown in Fig. 9. As shown in the Figure, the critical temperature, T_c, of the Prussian blue is about 4.2 K. When the Prussian blue is reduced, T_c progressively reduces. This modification of the magnetic properties arises mainly from a change in the degree of the valence delocalization. The electrons in the Prussian blue formally occupying the t_{2g} orbitals on the $Fe^{II\text{-}LS}(t^6_{2g}e^0_g)$ are partly delocalized onto the neighboring $Fe^{III\text{-}HS}(t^3_{2g}e^2_g)$. Since the t_{2g} and e_g orbitals of the $Fe^{III\text{-}HS}$ are both exactly half occupied, it is energetically favorable to delocalize only one type of spin (α or β spin) from the $Fe^{II\text{-}LS}$ to the $Fe^{III\text{-}HS}$ due to the coulomb and exchange repulsion terms.[60] The spin polarization on the $Fe^{II\text{-}LS}$ induces a magnetic correlation between the $Fe^{III\text{-}HS}$, leading to magnetic ordering at 4.2 K. On the other hand, after reduction, the electronic state is converted to $Fe^{II\text{-}LS}(t^6_{2g}e^0_g)$-CN-$Fe^{II\text{-}HS}(t^4_{2g}e^2_g)$ and hence the partial delocalization of the electrons from the $Fe^{II\text{-}LS}$ to the $Fe^{II\text{-}HS}$ (or vice versa) is prevented due to a large coulomb-repulsion. Thus, the spin polarization on the $Fe^{II\text{-}LS}$ almost disappears, which results in the reduction of the magnetic interaction between the $Fe^{II\text{-}HS}$ through the $Fe^{II\text{-}LS}$. As a consequence, the compound shows ferromagnetic to paramagnetic interconversion by electrochemical reduction. Furthermore, when the Prussian blue is oxidized to $Fe^{III}_4[Fe^{III}(CN)_6]_3(Cl)_3$, the T_c progressively increases. This is consistent with the fact that the diamagnetic component, $Fe^{II\text{-}LS}(t^6_{2g}e^0_g)$, is oxidized to $Fe^{III\text{-}LS}(t^5_{2g}e^0_g)$ with one unpaired electron

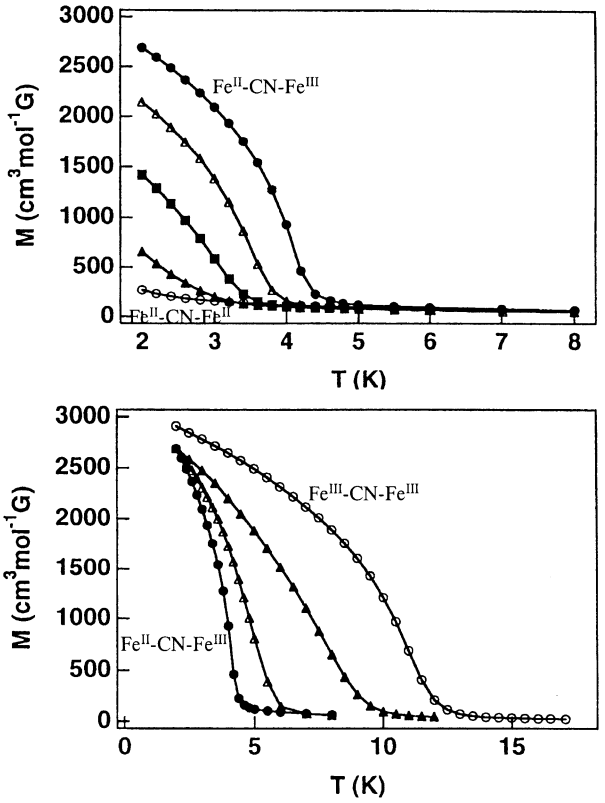

Fig. 9. Change in the critical temperature during electrochemical reduction from the Fe^{II}-CN-Fe^{III} form to the Fe^{II}-CN-Fe^{II} form (top), and during electrochemical oxidation from the Fe^{II}-CN-Fe^{III} form to the Fe^{III}-CN-Fe^{III} form (bottom). Solid lines serve to guide the eye.

in the t_{2g} orbital. The electrochemical control of the magnetic properties in FeFe Prussian blue is schematically illustrated in Fig. 8.

2. Photoinduced Magnetization in FeCo Prussian Blue Analogues[6–18]

The control of magnetic properties using light has engendered a lot of interest because of its potential for a wide range of applications, from optical recording devices to photo-switchable magneto optical devices. However, in the photo-recording devices currently available, changes in the magnetic properties are induced by the photo-thermal mode rather than the photon mode, and hence the utility of these systems was quite limited. In order to access the materials at higher speed and with superior resolution, it would be preferable to control the magnetic properties by means of illumination. In order to achieve such optical switching, the compounds should have two nearly degenerate electronic states. Furthermore, in order to suppress the rapid relaxation back from the photo-induced metastable state, a strong molecular interaction should operate in these compounds.[25] To achieve this aim, we are focusing our work on FeCo Prussian blue (Fig. 1), where FeCo Prussian blue represents the Prussian blue analogues with Fe-CN-Co moieties. This is because of the proximity in electronic states between Fe^{II}-CN-$Co^{III\text{-}LS}$ and Fe^{III}-CN-$Co^{II\text{-}HS}$ in FeCo Prussian blue. The dinuclear FeCo complexes such as [(mta)Fe-CN-$Co(CN)_5]^-$ (mta = 10-methyl-1,4,8,12-tetraazacyclopentadecan-10-amine) and $[(NC)_5Fe\text{-}CN\text{-}Co(CN)_5]^{6-}$ have the Fe^{II}-CN-$Co^{III\text{-}LS}$ structure,[61–69] while $Co_{1.5}[Fe(CN)_6]$ has the Fe^{III}-CN-$Co^{II\text{-}HS}$ structure. Furthermore, a strong cooperativity is expected due to the three-dimensional CN network. This mechanism has the potential to extend the lifetime of the photo-excited state,[25] and we have in fact discovered that FeCo Prussian blue exhibits novel photo-magnetic effects.[6]

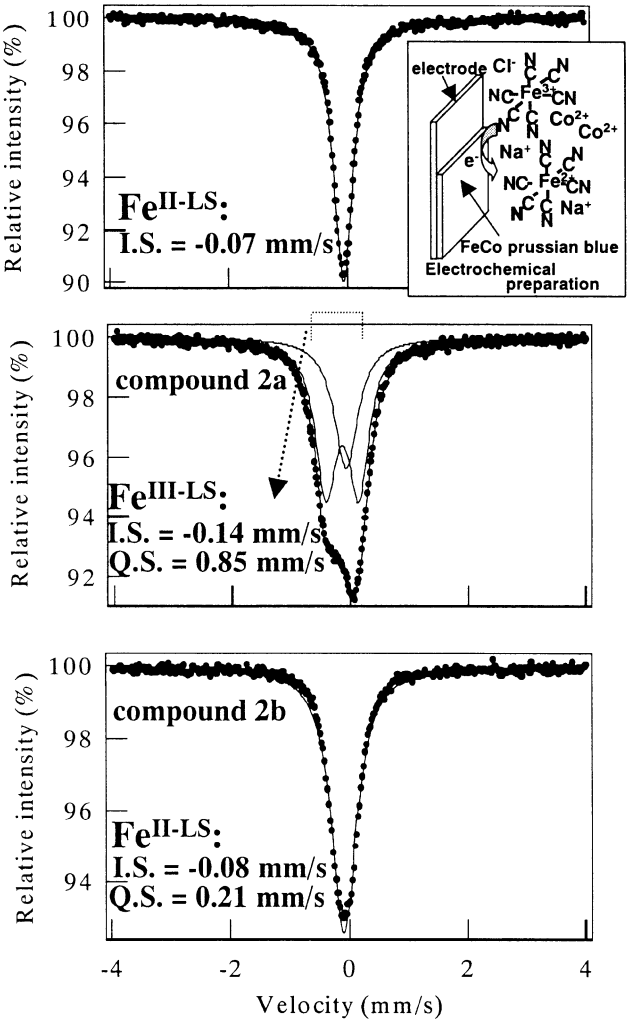

Fig. 10. (Top) Mössbauer spectra of electrochemically prepared FeCo Prussian blue with the Fe^{II}-CN-$Co^{II\text{-}HS}$ structure. Inset: schematic illustration of the electrochemical reduction technique for the preparation of the FeCo Prussian blue analogues. (Middle) Mössbauer spectra after electrochemical oxidation at 0.6V in 1 M NaCl solution. It should be noted that the spectrum shows the presence of a minor component consisting of Fe^{II} (I.S. = -0.06 mm s^{-1} and Q.S. = 0.04 mm s^{-1}).[79] (Bottom) Mössbauer spectra of **2b**, which is obtained by exchange of the alkali cation from Na^+ to K^+ in **2a**.

2-1. Electrochemical Preparation of FeCo Prussian blue with the Fe^{II}-CN-$Co^{II\text{-}HS}$ Structure. FeCo Prussian blue, $Na_{1.4}Co^{II\text{-}HS}{}_{1.3}[Fe^{II}(CN)_6]\cdot 5H_2O$ with the Fe^{II}-CN-$Co^{II\text{-}HS}$ structure, was synthesized on a Pt electrode by an electrochemical reduction technique (Fig. 10).[70–78] The procedure for this elec-

trochemical route is as follows. Two aqueous solutions, one containing 0.5 mM $Co^{II\text{-}HS}(NO_3)_2 \cdot H_2O$ and 1M $NaNO_3$ and one containing 0.5 mM $K_3[Fe^{III}(CN)_6]$ and 1 M $NaNO_3$ were prepared separately. The solutions were then mixed and then the electrochemical reduction was performed using a Pt electrode whilst vigorously bubbling the mixed solution with N_2 gas. The electrode potential was maintained at −0.4 V vs SCE. The electrochemical process can be expressed as follows:

$$[Fe^{III}(CN)_6]^{3-} + e^- \rightarrow [Fe^{II}(CN)6]4^-,$$
$$[Fe^{II}(CN)_6]^{4-} + 1.3Co^{II\text{-}HS} + 1.4Na^+ \rightarrow Na_{1.4}Co^{II\text{-}HS}{}_{1.3}[Fe^{II}(CN)_6].$$

That is, the $[Fe^{III}(CN)_6]^{3-}$ moieties are changed to relatively labile $[Fe^{II}(CN)_6]^{4-}$ compounds by an electrochemical reduction route on a Pt electrode. The generation of the labile species results in the formation of the Fe^{II}-CN-$Co^{II\text{-}HS}$ structure via a coordination reaction of the labile $[Fe^{II}(CN)_6]^{4-}$ moieties with $Co^{II\text{-}HS}$ ions. The reaction produced a green-coloured thin film of the FeCo Prussian blue compound $Na_{1.4}Co_{1.3}[Fe(CN)_6]\cdot 5H_2O$ (which has the Fe^{II}-CN-$Co^{II\text{-}HS}$ structure) on the Pt electrode. The ^{57}Fe Mössbauer spectrum showed a single peak with an isomer shift (I.S.) of −0.07 mm s^{-1}, which supports the view that the iron ions take the low-spin Fe^{II} state (Fig. 10). Note that the presence of the concentrated $NaNO_3$ is important in the electrochemical synthesis as presented here. This is because it suppresses the rapid precipitation of the FeCo Prussian blue with the Fe^{III}-CN-$Co^{II\text{-}HS}$ structure from the $[Fe^{III}(CN)_6]^{3-}$ and $Co^{II\text{-}HS}$ ions. Furthermore, it is important to note that the electrochemical synthesis should be performed immediately after the two solutions are mixed. This is because the precipitation reaction will gradually proceed anyway, even if the concentrated $NaNO_3$ is present, thereby preventing the formation of the FeCo thin film on the working Pt electrode.

2-2. Electrochemical Preparation of an Oxidized Form of the FeCo Prussian Blue; Alkali Cation Dependent Redox Reaction.[7,8] The oxidized forms of FeCo Prussian blue, $Na_{0.4}Co_{1.3}[Fe(CN)_6]\cdot 5H_2O$ (**2a**) and $K_{0.4}Co_{1.3}[Fe(CN)_6]\cdot 5H_2O$ (**2b**), were produced by electrochemically oxidizing the $Na_{1.4}Co^{II\text{-}HS}{}_{1.3}[Fe^{II}(CN)_6]\cdot 5H_2O$ complex, which has the Fe^{II}-CN-$Co^{II\text{-}HS}$ structure. The cyclic voltamogram in a 1 M NaCl aqueous solution is shown in Fig. 11. An oxidation peak is observed at 0.45 V vs SCE, and a small peak is observed at 0.8 V. An ^{57}Fe Mössbauer spectrum obtained after oxidation at 0.6 V shows that the single peak decreased significantly, and that a new doublet with an I.S. of −0.14 mm s^{-1} and a quadrupole splitting (Q.S.) of 0.85 mm s^{-1} appeared (Fig. 10).[79] This means that Fe^{II} is oxidized to low-spin Fe^{III} at 0.45 V. This view is supported by IR spectra (Fig. 12). This means that the electrochemical process in 1 M NaCl aqueous solution can be expressed as follows.

$$Na_{1.4}Co^{II\text{-}HS}{}_{1.3}[Fe^{II}(CN)_6] \rightarrow Na_{0.4}Co^{II\text{-}HS}{}_{1.3}[Fe^{III}(CN)_6] + Na^+ + e^-.$$

The peak at 0.8 V is due to the oxidation of $Co^{II\text{-}HS}$ ions (Fig. 11).

Similarly, electrochemical oxidation can be performed in a 1 M KCl aqueous solution. As shown in Fig. 12, the $Co^{II\text{-}HS}$ is oxidized first in KCl solution, which is distinguishable from the electrochemical oxidation reaction in NaCl solution.

Furthermore, it was found that dipping the FeCo Prussian blue thin film of **2a** into the KCl solution results in the exchange of the alkali cations, from Na^+ to K^+ ions. That is,

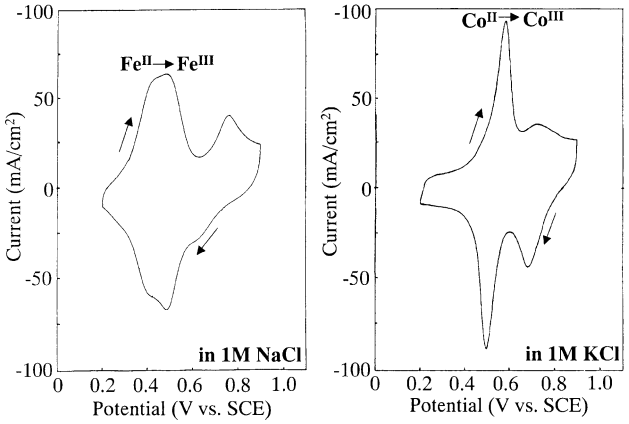

Fig. 11. Cyclic voltammogram of FeCo Prussian blue in 1 M NaCl aqueous solution (left) and 1M KCl aqueous solution (right).

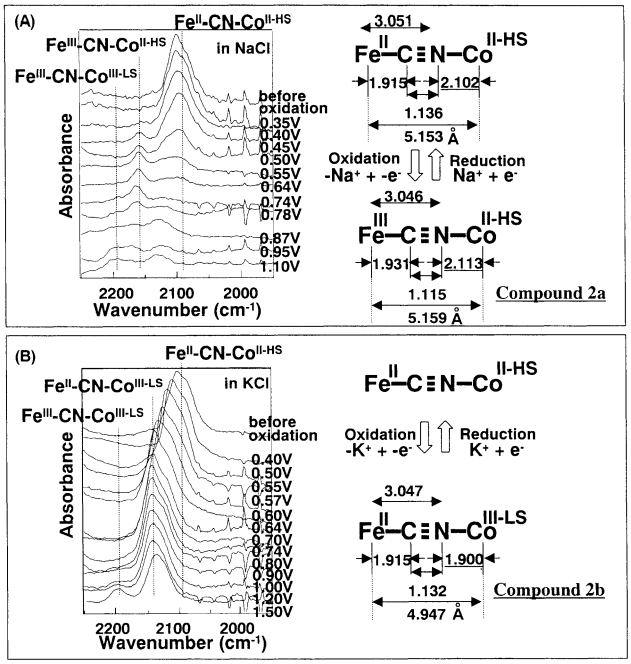

Fig. 12. IR spectra during electrochemical oxidation in 1 M NaCl solution (A) and 1 M KCl solution (B), and schematic illustration of the change in the oxidation state during the electrochemical redox reaction in the 1 M NaCl and KCl solutions. The peaks at 2090, 2160 and 2200 cm^{-1} can be assigned to the ν(CN) with the Fe^{II}-CN-$Co^{II\text{-}HS}$, Fe^{III}-CN-$Co^{II\text{-}HS}$ and Fe^{III}-CN-$Co^{III\text{-}LS}$ structures, respectively. This means that Fe^{II} is oxidized first in 1 M NaCl solution. On the other hand, the ν(CN) peak shifts from 2090 to 2130 cm^{-1} in KCl solution. The absorption at 2130 cm^{-1} can be assigned to the ν(CN) with Fe^{II}-CN-$Co^{III\text{-}LS}$ structure. This implies that the $Co^{II\text{-}HS}$ is oxidized first in KCl solution.

when the Pt electrode coated with the red thin film of FeCo Prussian blue, ($Na_{0.4}Co^{II\text{-}HS}{}_{1.3}[Fe^{II}(CN)_6]\cdot 5H_2O$ with the Fe^{III}-CN-$Co^{II\text{-}HS}$ structure), was dipped into the 1 M KCl aqueous solution for a few minutes, the color changed from red to purple. The IR spectra show that the CN stretching peak shifts from 2160 to 2130 cm^{-1}. The Mössbauer spectra exhibited an I.S. of -0.08 mm s^{-1} and Q.S. of 0.21 mm s^{-1}, indicating the presence of low-spin Fe^{II} (Fig. 10).[79] This means that the following ion exchange reaction proceeded during the dipping process:

$$Na_{0.4}Co^{II\text{-}HS}{}_{1.3}[Fe^{III}(CN)_6] + 0.4K^+ \rightarrow K_{0.4}Co^{II\text{-}HS}{}_{0.3}Co^{III\text{-}LS}[Fe^{II}(CN)_6] + 0.4Na^+.$$

Consequently, two kinds of photo-magnetic FeCo Prussian blue can be obtained, i.e. $Na_{0.4}Co^{II\text{-}HS}{}_{1.3}[Fe^{III}(CN)_6]\cdot 5H_2O$ (**2a**) and $K_{0.4}Co^{II\text{-}HS}{}_{0.3}Co^{III\text{-}LS}[Fe^{II}(CN)_6]\cdot 5H_2O$ (**2b**).

2-3. Structure of the FeCo Prussian Blue at Room Temperature. The powder X-ray diffraction patterns of the present compound are consistent with the fcc structure. The unit cell parameters of compounds **2a** and **2b** are 10.32 Å and 9.96 Å, respectively.

The local structures around the Fe and Co atoms were determined from the Fe and Co K-edge extended X-ray-absorption fine structure spectra (EXAFS).[17] It is confirmed that the local structure around the Fe is $Fe(CN)_6Co_6$, while around the Co it is $Co(NC)_{6-y}(H_2O)_yFe_{6-y}$. The Fe–C, Fe–N, C–N and Co–N,O distances at 296 K for compounds **2a** and **2b** are shown in Fig. 12. The Fe–C, Fe–N and C–N distances do not significantly change between **2a** and **2b**. On the other hand, the first nearest neighbor Co–N,O distances are noticeably different between the Co^{II} and Co^{III} complexes. The dominant Co valence in **2a** at 296 K is Co^{II}. The Co^{II}–N,O distance at 296 K for **2a** is 2.113 Å (Fig. 12). On the other hand, the Co valence in **2b** at 296 K is mainly Co^{III}. The Co^{III}–N,O distance at 296 K for **2b** is 1.900 Å (Fig. 12). These results show that the change in the unit cell parameters (10.32 Å to 9.96 Å) deduced from the powder X-ray measurements is mainly due to the variation in the Co–N,O bond length.

2-4. Thermally Induced Electron Transfer between Fe and Co. The products of the molar magnetic susceptibility and temperature, $\chi_M T$, as a function of temperature are shown for compounds **2a** and **2b** in Fig. 13.

The $\chi_M T$ product of compound **2a** at 300 K is ca. 4 cm^3 mol^{-1} K, which is consistent with the presence of Fe^{III}-CN-$Co^{II\text{-}HS}$. On cooling it abruptly decreases at 260 K and reaches 1.0 cm^3 mol^{-1} K at 20 K, indicating the presence of Fe^{II}-CN-$Co^{III\text{-}LS}$. These results show that the following electron transfer between $Co^{II\text{-}HS}$ and Fe^{III} is induced in **2a**,

$$Na_{0.4}Co^{II\text{-}HS}{}_{1.3}[Fe^{III}(CN)_6] \rightarrow Na_{0.4}Co^{II\text{-}HS}{}_{0.3}Co^{III\text{-}LS}[Fe^{II}(CN)_6].$$

The Mössbauer (Fig. 14) and IR spectra (Fig. 15) confirm the thermally induced electron transfer. The phase transition could also be detected by UV-vis absorption spectra (Fig. 16). Note that the color of the FeCo compounds with the Fe^{III}-CN-$Co^{II\text{-}HS}$ structure is red and the color of those with the Fe^{II}-CN-$Co^{III\text{-}LS}$ structure is purple (Fig. 17).

On the other hand, the $\chi_M T$ product of compound **2b** is nearly constant as a function of temperature below 340 K. Correspondingly, little temperature dependence was observed for both the Mössbauer spectra and the ν(CN) peaks at 2125 cm^{-1}

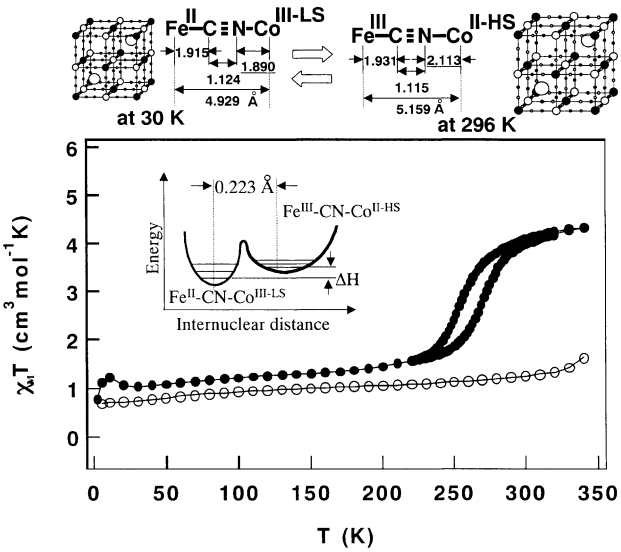

Fig. 13. (Top) Change in the bond distance of **2a** between 296 K and 30 K, which is determined from the Fe and Co *K*-edge EXAFS. The difference in the Co–N,O distance (0.223 Å) is due to the e_g σ-antibonding orbitals in the $Co^{III\text{-}LS}(t_{2g}^6e_g^0)$ form being unoccupied, whilst they are doubly occupied in the $Co^{II\text{-}HS}(t_{2g}^5e_g^2)$ form. (Bottom) Temperature dependence of the magnetization of compounds **2a** (●) and **2b** (○). An electron transfer between $Co^{II\text{-}HS}$ and Fe^{III} is induced in **2a** at around 260 K. The presence of a hysteresis loop indicates that the phase transition has a first order character.

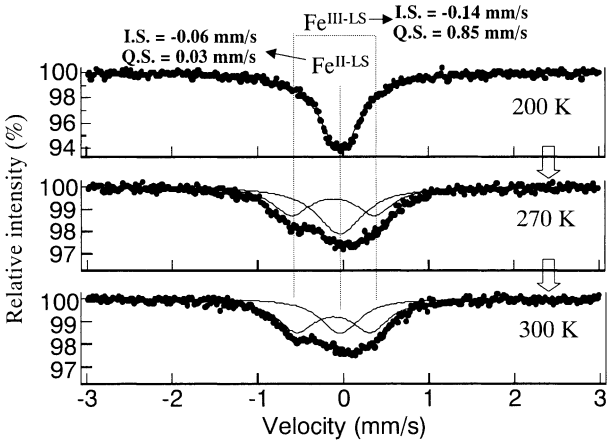

Fig. 14. The ^{57}Fe Mössbauer spectra of **2a** measured at 200 K, 270 K and 300 K in the heating mode. The intense peak in the spectrum at 200 K is characteristic of the state where I.S. = -0.06 mm s^{-1} and Q.S. = 0.03 mm s^{-1}, which can be assigned to $Fe^{II\text{-}LS}$. At 270 K, an outside doublet becomes visible. The Mössbauer parameters of the outside doublet at 300 K are I.S. = -0.14 mm s^{-1} and Q.S. = 0.85 mm s^{-1}, which can be assigned to $Fe^{III\text{-}LS}$. It is thus demonstrated that compound **2a** undergoes a change in its electronic state from $Fe^{II\text{-}LS}$ to $Fe^{III\text{-}LS}$.

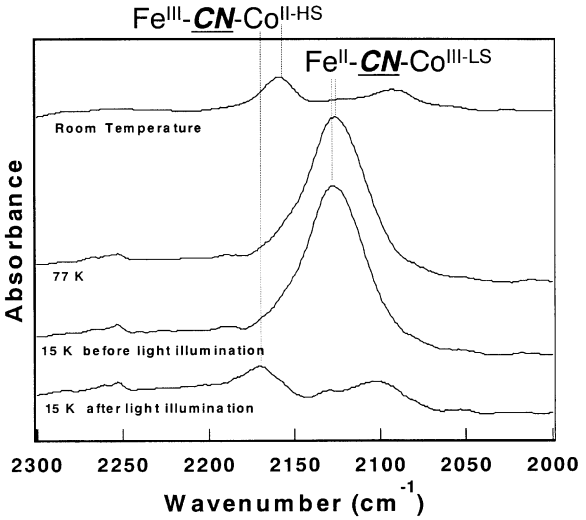

Fig. 15. IR spectra of **2a** at room temperature, 77 K and 15 K before illumination and at 15 K after illumination. On cooling, the ν(CN) peak at ca. 2160 cm^{-1} (which is ascribable to Fe^{III}-CN-$Co^{II\text{-}HS}$) shifted to ca. 2125–2130 cm^{-1} (ascribable to Fe^{II}-CN-$Co^{III\text{-}LS}$). This means that an electron is transferred from $Co^{II\text{-}HS}$ to Fe^{III}. Furthermore, after illumination, a ν(CN) peak appeared at 2162 cm^{-1} in the Fe^{III}-CN-$Co^{II\text{-}HS}$ structure, and the ν(CN) peak at ca. 2130 cm^{-1} in the Fe^{II}-CN-$Co^{III\text{-}LS}$ structure nearly disappeared.

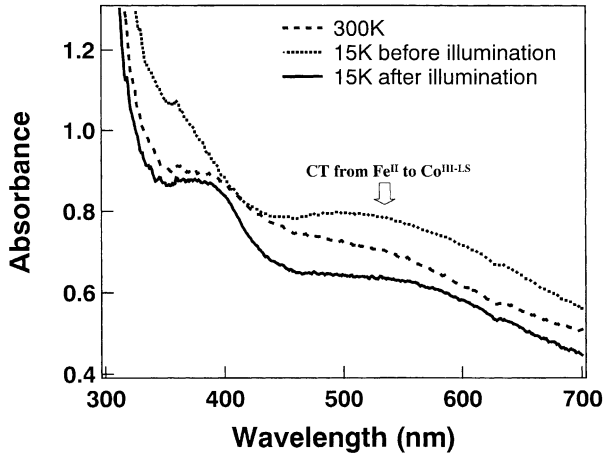

Fig. 16. UV-vis absorption spectra of **2a** at 300 K and at 15 K before and after illumination. The absorption at 550 nm decreased and a peak appeared at around 400 nm after visible light illumination.

for compound **2b**. The Mössbauer spectra for compound **2b** shows a peak (I.S. = −0.08 ∼ −0.04 mm/s) that can be assigned to $Fe^{II\text{-}LS}$, that is, the electronic state of compound **2b** is Fe^{II}-CN-$Co^{III\text{-}LS}$ below 340 K.

2-5. Structural Difference of the FeCo Prussian Blue between 30 K and Room Temperature. The local structures around the Fe and Co atoms at 30 K were determined from the Fe and Co *K*-edge EXAFS results. The bond distances of **2a** are shown in Fig. 13. This shows that there are no appreciable changes in the Fe–C, Fe–N and C–N distances between 296 K and 30 K. On the other hand, a large change is observed in the

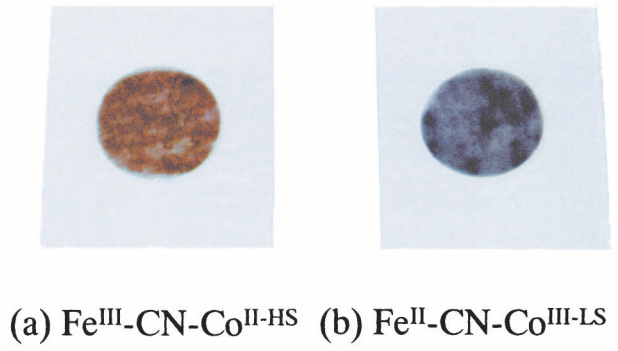

Fig. 17. Color of the FeCo Prussian blue with the (a) Fe^{III}-CN-$Co^{II\text{-}HS}$ and (b) Fe^{II}-CN-$Co^{III\text{-}LS}$ structure.

Co–N,O distance. The dominant Co valence in **2a** at 30 K is $Co^{III\text{-}LS}$. The EXAFS spectra show that the $Co^{III\text{-}LS}$–N,O distance at 30 K is 1.890 Å. This means that the Co–N,O distance changed from 2.113 Å ($Co^{II\text{-}HS}$–N,O) at 293 K to 1.890 Å ($Co^{III\text{-}LS}$–N,O) at 30 K. The change in the bond length (Co–N,O), Δr, is 0.223 Å, which is consistent with that of Co valence tautomeric compounds.[80]

On the other hand, there are no appreciable changes in the Co–N,O, Fe–C, Fe–N and C–N distances between 296 K and 30 K for **2b**. This is because **2b** exhibits no phase transition involving electron transfer. Note that the bond distances of **2b** at 30 K are 1.909, 3.034, 1.125 and 1.894 Å for the Fe–C, Fe–N, C–N and $Co^{III\text{-}LS}$–N,O distances respectively.

2-6. Mechanisms for Switching between the Ground State and the Metastable State. The parameter that we need to consider in order to define the lowest energy state is the Gibbs free energy, G, which takes into account the entropy factor S in addition to the enthalpy factor H. The thermal population of the tautomeric states between the Fe^{III}-CN-$Co^{II\text{-}HS}$ (= $Fe^{III}Co^{II}$) state and the Fe^{II}-CN-$Co^{III\text{-}LS}$ (= $Fe^{II}Co^{III}$) state is dictated by the Gibbs free energy difference,

$$\Delta G = \Delta H - T\Delta S,$$

where $\Delta G = G_{Fe^{III}Co^{II}} - G_{Fe^{II}Co^{III}}$, $\Delta H = H_{Fe^{III}Co^{II}} - H_{Fe^{II}Co^{III}}$ and $\Delta S = S_{Fe^{III}Co^{II}} - S_{Fe^{II}Co^{III}}$. The critical temperature T_c of the phase transition is defined by $\Delta G = \Delta H - T\Delta S = 0$. Hence,

$$T_c = \Delta H/\Delta S.$$

The entropy variation, ΔS, neglecting the intermolecular interaction, may be written as the sum of the electronic ΔS_{el} and the vibrational ΔS_{vib} contributions:

$$\Delta S = \Delta S_{el} + \Delta S_{vib}.$$

ΔS_{el} may contain contributions from both spin (ΔS_{el}^{spin}) and orbital (ΔS_{el}^{orb}) degeneracy.

$$\Delta S_{el} = \Delta S_{el}^{spin} + \Delta S_{el}^{orb}$$

However, in the case that we are interested in, orbital degeneracy is mostly removed because of the low actual symmetry, and then

$$\Delta S_{el} = \Delta S_{el}{}^{spin} = R\ln(\omega_{Fe^{III}Co^{II}}/\omega_{Fe^{II}Co^{III}}),$$

where $\omega_{Fe^{III}Co^{II}}$ and $\omega_{Fe^{II}Co^{III}}$ are the number of spin configurations (i.e., spin multiplicity) for the Fe^{III}-CN-$Co^{II\text{-}HS}$ state and Fe^{II}-CN-$Co^{III\text{-}LS}$ state, respectively. Hence, ΔS_{el} is positive. The other major contribution to ΔS arises from changes in the phonon modes, i.e. ΔS_{vib}. As is described in Section 2–5, the first nearest neighbor Co–N,O distances are noticeably different between the $Co^{III\text{-}LS}$ and $Co^{II\text{-}HS}$ complexes, i.e. 1.890 Å and 2.113 Å, respectively. This means that vibrational disorder is more pronounced in the Fe^{III}-CN-$Co^{II\text{-}HS}$ state than in the Fe^{II}-CN-$Co^{III\text{-}LS}$ state, owing to the longer Co-ligand bond length. Hence, ΔS_{vib} is positive, which results in $\Delta S = \Delta S_{el} + \Delta S_{vib} > 0$. In order for T_c to be positive, ΔH and ΔS must have the same sign. Hence, in the present case, $\Delta H = H_{Fe^{III}Co^{II}} - H_{Fe^{II}Co^{III}}$ should be positive. This means that the minimum of the Fe^{II}-CN-$Co^{III\text{-}LS}$ potential energy is slightly lower than the minimum of the Fe^{III}-CN-$Co^{II\text{-}HS}$ potential energy. The energy curve is shown in Fig. 13. Below T_c, the enthalpy factor dominates and hence the Fe^{II}-CN-$Co^{III\text{-}LS}$ state is the most stable one. On the other hand, above T_c, the entropy factor dominates and hence the Fe^{III}-CN-$Co^{II\text{-}HS}$ state is the most stable one. The observed thermally induced phase transition is entropy driven.

2-7. Photo-Induced Magnetization. The existence of two minima in the potential energy curves, with the Fe^{II}-CN-$Co^{III\text{-}LS}$ state being lower in energy than the Fe^{III}-CN-$Co^{II\text{-}HS}$ state, has allowed the observation of photoinduced magnetization effects. The absorption spectra of the compounds $Na_{0.4}Co^{II\text{-}HS}{}_{0.3}Co^{III\text{-}LS}[Fe^{II}(CN)_6]$ [low-temperature phase of (**2a**)] and $K_{0.4}Co^{II\text{-}HS}{}_{0.3}Co^{III\text{-}LS}[Fe^{II}(CN)_6]$ (**2b**) show a broad absorption band around 550 nm (Fig. 16). This band can be attributed to a charge transfer (CT) from Fe^{II} to $Co^{III\text{-}LS}$. This assignment is consistent with the CT bands reported for binuclear species with the Fe^{II}-CN-$Co^{III\text{-}LS}$ structure.[61–69] Furthermore, this is confirmed by the first principles band calculations (Fig. 18). Kawamoto et al. have reported that the main component of the highest occupied molecular orbital (HOMO) is the $d\varepsilon$ orbital of Fe, and that the lowest unoccupied molecular orbital (LUMO) is the $d\gamma$ orbital of Co.[81] Hence, the absorption is due to a CT from Fe to Co. The energy difference is about 1.4 eV. This is slightly smaller than the observed absorption peak, which is a general tendency of the local density approximation.

The photo-magnetic properties of compound **2a** and **2b** were investigated with a superconducting quantum interference device (SQUID) magnetometer. Filtered visible light (500–750 nm, 10 mW/cm^2) from the Hg-Xe lamp was used to excite the CT band from $Co^{II\text{-}HS}$ to Fe^{III}. When the sample was illuminated at 5 K with visible light guided via an optical fiber into the SQUID magnetometer, an increase in the magnetization value could be observed at 5 G. The FCM plots measured as a function of temperature after illumination for 10 minutes showed an abrupt break around 26 K (Fig. 19). The magnetization (M) versus magnetic field (H) was measured at 2 K. The plot of M vs H before illumination did not show any hysteresis loops, since it is a paramagnetic compound. In contrast, the plot of M vs H after illumination did exhibit hysteresis loops (Fig. 20). The field dependence of the magnetization at 2 K showed that the magnetization value was significantly increased after illumination (Fig. 20). These results demonstrate that the paramagnetic material was converted to a magnetic material by illumination. When the temperature of the sample was raised to 150 K, the magnetic properties quickly relaxed to almost the initial state. It should be noted that Pejakovic et al.

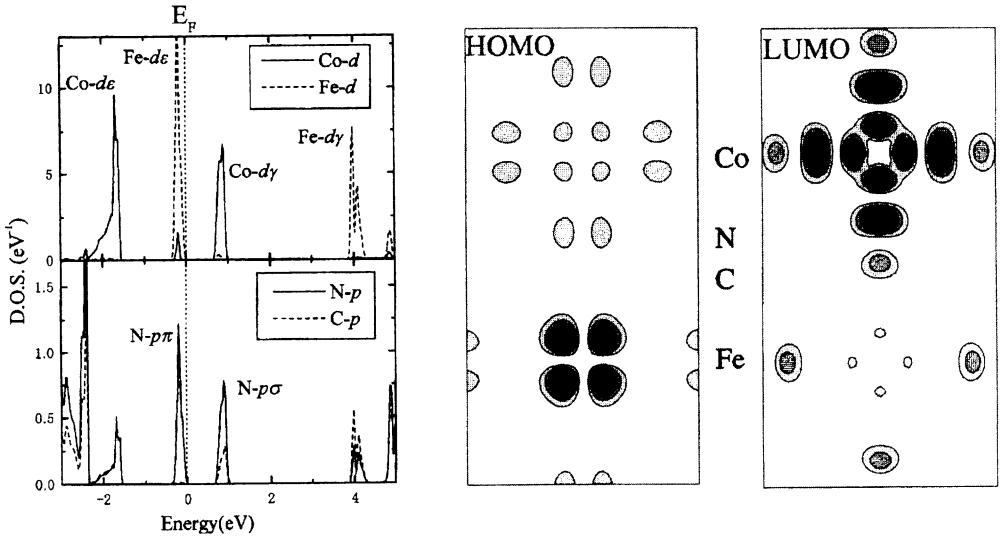

Fig. 18. (Left) Local density of states of $CoFe(CN)_6$ in each muffin tin sphere obtained with the ab initio band calculation. Reproduced with permission from Kawamoto et al.[81] (Right) Charge map of the Γ point of the LUMO band and the HOMO band. Reproduced with permission from Kawamoto et al.[81] The Fe-$d\varepsilon$ (HOMO) and the Co-$d\gamma$ (LUMO) orbitals are strongly connected with the N-$p\pi$ and N-$sp\sigma$ orbitals, respectively. The $d\varepsilon$ and $p\pi$ orbitals are antisymmetric, while the $d\gamma$ and $sp\sigma$ orbitals are symmetric. A high probability of the optical dipole transition between HOMO and LUMO occurring is expected due to the component on the nitrogen atoms, because the transition between the N-$p\pi$ and N-$sp\sigma$ orbitals satisfies the selection rule. As a result, optical absorption accompanied by the charge transfer between Co and Fe is observed.[191]

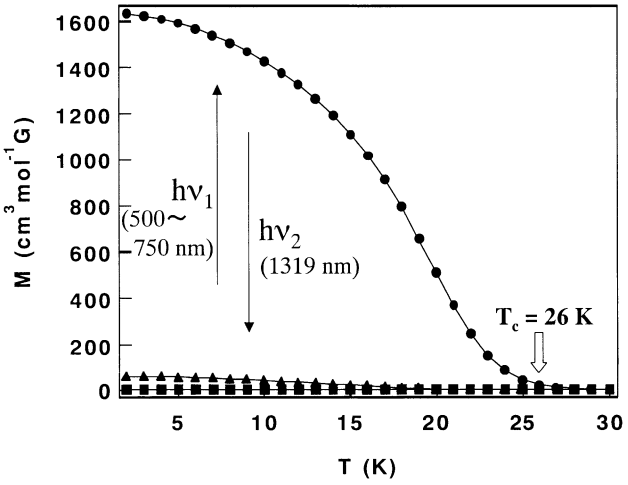

Fig. 19. Field-cooled magnetization vs temperature curves of **2b** at $H = 5$ G (■) before light illumination; (●) after visible light ($h\nu_1$) illumination; (▲) after near-IR light ($h\nu_2$) illumination. No magnetic phase transition can be observed before illumination, because the main components in **2b** are the diamagnetic Fe^{II} and $Co^{III\text{-}LS}$ moieties. On the other hand, the FCM plots after visible light illumination showed an abrupt break around 26 K, i.e. $T_c = 26$ K. Furthermore, the enhancement of the magnetization could almost be reverted back to the original level by near-IR light illumination.[7]

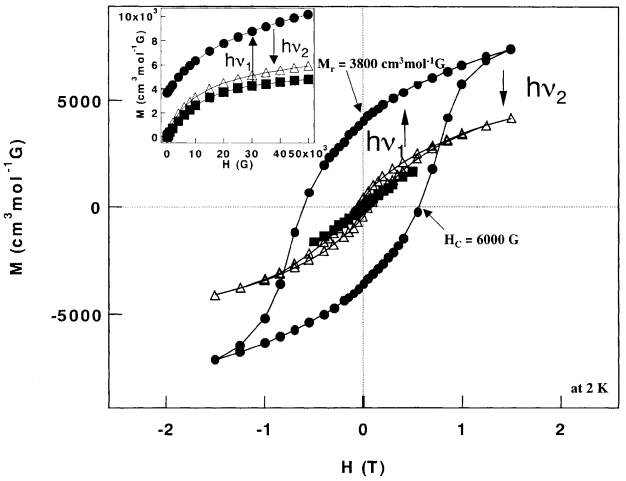

Fig. 20. Hysteresis loops of **2b** at 2 K (■) before light illumination; (●) after visible light ($h\nu_1$) illumination; (△) after near-IR light ($h\nu_2$) illumination.[7] Inset: Field dependence of the magnetization at 2 K (■) before light illumination; (●) after visible light ($h\nu_1$) illumination; (△) after near-IR light ($h\nu_2$) illumination.

have recently carried out a dynamic susceptibility study of the FeCo Prussian blue. They showed that the photoexcited state of $K_{1-2x}Co_{1+x}[Fe(CN)_6]\cdot yH_2O$ ($0.2 \leq x \leq 0.4$, $y \sim 5$) can be well described within a cluster glass model.[82–86]

^{57}Fe Mössbauer spectra (Fig. 21), IR (Fig. 15) and UV-vis spectra (Fig. 16) show that the change in the electronic states induced by light can be expressed as follows:

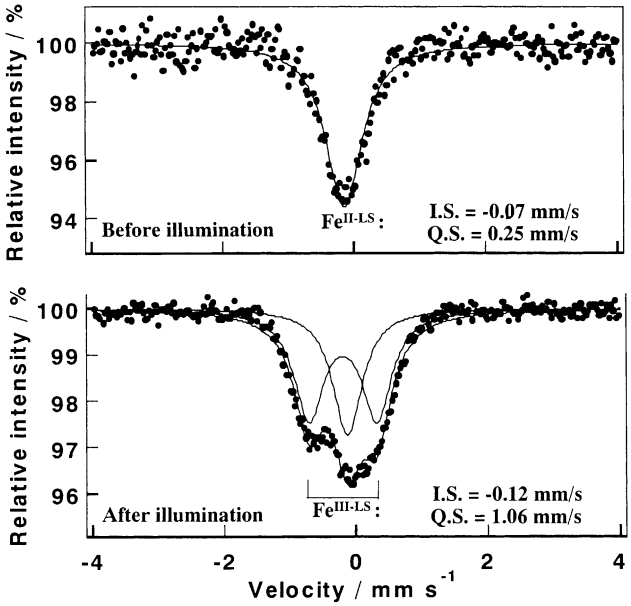

Fig. 21. Mössbauer spectra of compound **2b** at 30 K. (Top) before light illumination. (Bottom) after visible light illumination. The spectrum at 30 K before illumination has an absorption peak with I.S. = −0.07 mm/s, Q.S. = 0.25 mm/s, which is assigned to $Fe^{II\text{-}LS}$. On the other hand, a new doublet absorption peak with I.S. = −0.12 mm/s and Q.S. = 1.06 mm/s appeared after visible light illumination (400–700 nm, 100 mW/cm^2, 10 min.). The peak is assigned to $Fe^{III\text{-}LS}$. Note that, when the change reaches saturation, the Fe^{II}/Fe^{III} ratio after illumination was 35/65 under the present experimental conditions.

$$Fe^{II}(t_{2g}{}^6e_g{}^0)\text{-}CN\text{-}Co^{III\text{-}LS}(t_{2g}{}^6e_g{}^0) \rightarrow Fe^{III}(t_{2g}{}^5e_g{}^0)\text{-}CN\text{-}Co^{II\text{-}HS}(t_{2g}{}^5e_g{}^2).$$

That is, the following photo-reaction proceeds.

$$A_{0.4}Co^{II\text{-}HS}{}_{0.3}Co^{III\text{-}LS}[Fe^{II}(CN)_6] \rightarrow A_{0.4}Co^{II\text{-}HS}{}_{1.3}[Fe^{III}(CN)_6],$$

where A represents Na^+ or K^+. Similar photomagnetic properties were observed for Rb^+ and Cs^+ salts.[9,87–93]

The magnetic interaction between Fe and Co after illumination is expected to be anti-ferromagnetic. There are two types of exchange interactions operating in the present compound. The interaction between the t_{2g} orbital of Fe^{III} and the e_g orbital of the $Co^{II\text{-}HS}$ are ferromagnetic, while the interaction between the t_{2g} orbital of Fe^{III} and t_{2g} orbital of the $Co^{II\text{-}HS}$ gives rise to antiferromagnetic character. When the ferromagnetic and antiferromagnetic interactions are superimposed, the antiferromagnetic term dominates the interactions. Therefore, the magnetic properties after illumination are dominantly ferrimagnetic. This is consistent with the observation that the magnetic properties of a related compound, $Co^{II\text{-}HS}{}_{1.5}[Fe^{III}(CN)_6]\cdot 6H_2O$, are ferrimagnetic in character.

It is important to note that Champion et al. have measured the X-ray magnetic circular dichromism (XRD) at the Co and Fe *K* edges and have presented direct experimental evidence of the antiferromagnetic interaction between the Co and Fe

ions.[94]

2-8. Structural Changes Induced by Light. Yokoyama et al. have measured the local structures around the Fe and Co atoms before and after illumination at 36 K for $Na_{0.4}Co_{1.3}$-$[Fe(CN)_6]\cdot 5H_2O$ using Fe and Co *K*-edge XANES (X-ray-absorption near-edge structure) and EXAFS spectra (Fig. 22).[18] They show that there are no appreciable changes in the Fe–C, Fe–N and C–N distances before and after illumination. On the other hand, large changes are observed for the oxidation state of the Co and for the Co–N,O distance. Before illumination, the $Co^{III\text{-}LS}$ ratio, i.e. $[Co^{III\text{-}LS}/(Co^{II\text{-}HS} + Co^{III\text{-}LS})]$, was found to be 0.708, which is close to the ideal value for the low temperature phase (0.769). After illumination, the $Co^{III\text{-}LS}$ ratio was reduced to 0.168. This is consistent with the electron transfer from Fe^{II} to $Co^{III\text{-}LS}$. Furthermore, the Co–N,O distance changed from 1.89 Å ($Co^{III\text{-}LS}$–N,O) to 2.11 Å ($Co^{II\text{-}HS}$–N,O)(Fig. 23). This means that the local structure of the trapped photoexcited state was almost identical with that of the high-temperature phase.

Recently, Moulin et al. have investigated the local structure

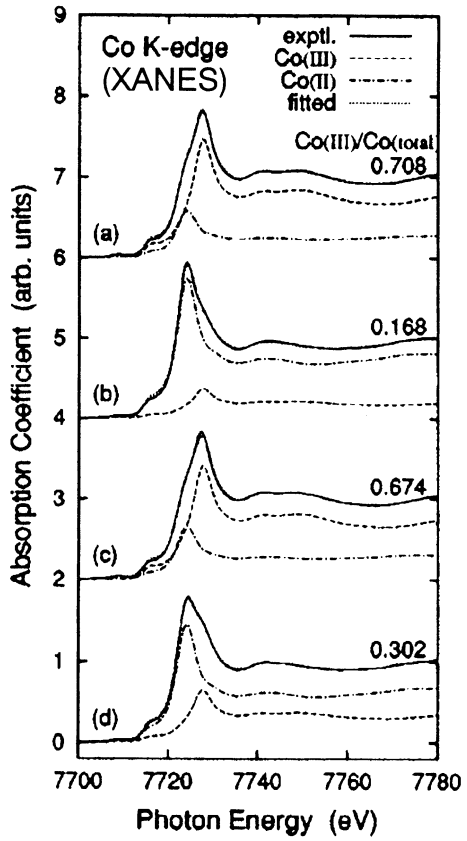

Fig. 22. Experimental Co *K*-edge XANES spectra (solid line) of **2a** in the sequential visible-light irradiation experiments: (a) before illumination at 36 K, (b) after illumination at 36 K, (c) heating the irradiated sample to 150 K, and (d) subsequent heating to 300 K. In the Co *K*-edge spectra, the results of the factor analysis are also given. The Co^{III} composition ratio is given numerically, and the estimated pure Co^{II} and Co^{III} spectra are plotted as dot-dashed and dashed lines, respectively, where the edge jumps correspond to the composition ratios.[18]

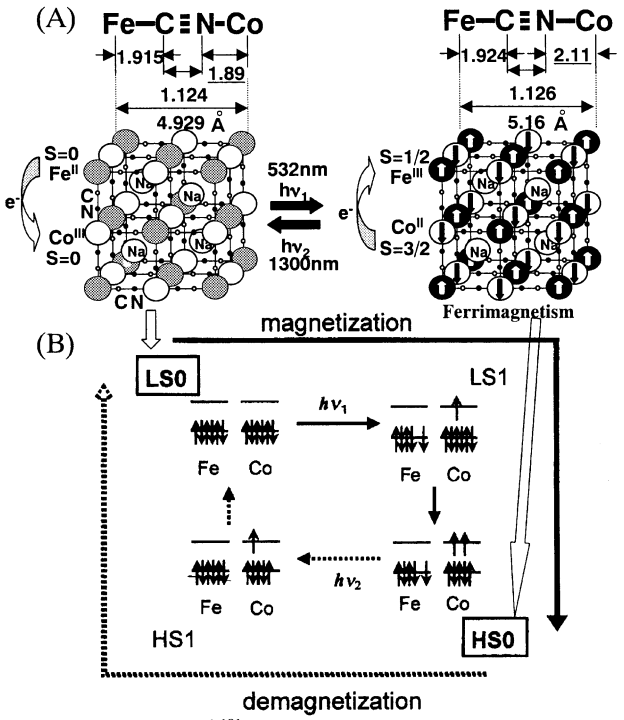

T. Kawamoto et al.[101]

Fig. 23. (A) Schematic illustration of the changes in the structure and the electronic states induced by visible light and near-IR light illumination. (B) Paths for the reversible photoinduced transition in the FeCo Prussian blue.[101] LS0, HS0, LS1 and HS1 represent the non-magnetic ground state, the magnetic metastable state, the paramagnetic excited state and the magnetic excited state, respectively. $h\nu$ indicates a photo-excited charge transfer. Reproduced with permission from Kawamoto et al.[101]

of the excited state and the ground state in a related compound, $Rb_{1.8}Co^{II\text{-}HS}{}_4[Fe^{III}(CN)_6]_{3.3}\cdot 13H_2O$, by XANES and EXAFS.[95] Their measured spectra evidence a local electronic transfer and a spin change induced by illumination in the Co ions.

2-9. Photo-Induced Demagnetization. The metastable compound has absorption bands around 400 nm and 1300 nm, respectively. Hence, by selectively illuminating those absorption bands, a reverse electron transfer from $Co^{II\text{-}HS}$ to Fe^{III} might be induced. In fact, when the sample was illuminated by near-IR light (1319 nm, 2.5 mW/cm^2) with a YAG laser, a decrease in the magnetization value was observed. The FCM plots measured as a function of temperature after illumination for 10 hours at 5 K showed that the enhancement of the magnetization resulting from visible light illumination can be almost completely reverted back to the original condition (Fig. 19). Furthermore, the hysteresis loop almost completely disappeared (Fig. 20). IR spectra showed that the CN stretching peak at 2162 cm^{-1} decreased and that a peak at around 2130 cm^{-1} increased after near-IR illumination. This indicates that the following reverse process is induced:

$$Fe^{II}(t_{2g}{}^6e_g{}^0)\text{-CN-}Co^{III\text{-}LS}(t_{2g}{}^6e_g{}^0) \leftarrow Fe^{III}(t_{2g}{}^5e_g^0)\text{-CN-}Co^{II\text{-}HS}(t_{2g}{}^5e_g{}^2).$$

That is,

$$A_{0.4}Co^{II\text{-}HS}{}_{0.3}Co^{III\text{-}LS}[Fe^{II}(CN)_6] \leftarrow A_{0.4}Co^{II\text{-}HS}{}_{1.3}[Fe^{III}(CN)_6]$$

This shows that the magnetic properties of thin films of FeCo Prussian blue can be switched between paramagnetic and ferrimagnetic via light illumination.

2-10. Theoretical Aspects. The photomagnetic properties have been studied from a theoretical viewpoint by several groups.[51,81,96–102] Here, we briefly introduce the mechanism reported by Kawamoto et al.[81,100–102] In order to discuss the tendencies of local structural changes, they calculated the energies of four different states (Fig. 23). The energy difference Δ(Fe) between the two spin states Fe^{II} and Fe^{III} was assumed to be 0.4 eV, and quantum-chemical ab initio calculations were carried out on three clusters, which had a cobalt atom at the center surrounded by ligands, by varying the bond length d(Co–N). The three clusters are (a) $Co(NC)_6$ (N_w = 0), (b) $Co(NC)_5{\cdot}H_2O$ (N_w = 1) and (c) $Co(NC)_4{\cdot}2H_2O$ (N_w = 2). The clusters (a), (b) and (c) correspond to those with zero, one and two $[Fe(CN)_6]$ vacancies in the six nearest neighbor iron sites. N_w denotes the number of water molecules in the cluster. The calculated results of the local potential of (a) and (b) are shown in Fig. 24. From the potential diagrams, they conclude that the photon energy for the transition of $Fe^{II}(t_{2g}{}^6e_g{}^0)$-CN-$Co^{III\text{-}LS}$-$(t_{2g}{}^6e_g{}^0)$ → $Fe^{III}(t_{2g}{}^5e_g{}^0)$-CN-$Co^{II\text{-}HS}(t_{2g}{}^5e_g{}^2)$ corresponds to the CT excitation on the cluster $Co(NC)_5{\cdot}H_2O$ (N_w = 1). On the other hand, they also conclude that the near-IR light for $Fe^{III}(t_{2g}^5e_g^0)$-CN-$Co^{II\text{-}HS}(t_{2g}^5e_g^0)$ → $Fe^{II}(t_{2g}^6e_g^0)$-CN-$Co^{III\text{-}LS}(t_{2g}^6e_g^0)$ corresponds to the 0.8 eV Frank–Condon excitation energy of the cluster $Co(NC)_6$ (N_w = 0). It is thought that when the created CT excitons (relaxed CT state) are accumulated in the compounds, the surrounding lattice around the excitons eventually undergoes a global change as an integration of all the local changes.[102]

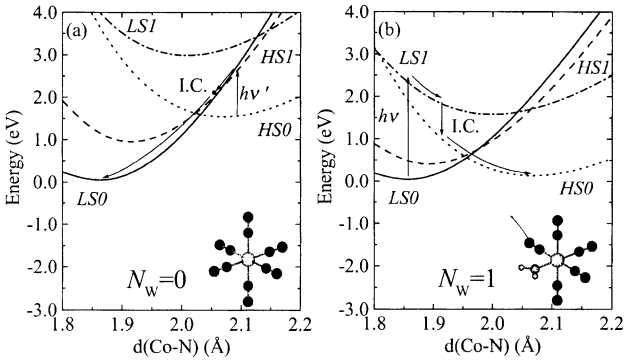

Fig. 24. Calculated local potentials of the two cobalt-centered clusters: (a) N_W = 0; (b) N_W = 1.[101] The solid line, the broken-dotted line, the dotted line and the broken line denote LS0, LS1, HS0 and HS1, respectively. Possible primary relaxation paths for the LS0 → HS0 and HS0 → LS0 transitions are indicated schematically by arrows in (b) and (a). Reproduced with permission from Kawamoto et al.[101]

2-11. Chemical Tuning of Phase Transition Temperature. The Prussian blue analogues present intrinsic $[Fe(CN)_6]$ vacancies due to their stoichiometry. The vacancy at the $[Fe(CN)_6]$ site is surrounded by six water molecules, which coordinate to the Co ions (Fig. 1). The insertion of alkali cations in the tetrahedral sites of the structure is accompanied by the filling of the vacancies to ensure electro-neutrality. The ligand field for the nitrogen in the CN of $[Fe(CN)_6]$ is slightly higher than that for the oxygen in H_2O in the spectrochemical series. Hence, it is thought that the electronic state of Fe^{III}-CN-$Co^{II\text{-}HS}$ becomes more stable than that of Fe^{II}-CN-$Co^{III\text{-}LS}$ as the number of vacancies increases. In fact, $Co_{1.5}[Fe(CN)_6]{\cdot}6H_2O$ with a relatively weak ligand field of Co cations has the Fe^{III}-CN-$Co^{II\text{-}HS}$ state. This suggests that the control of the ligand field of Co cations by varying the number of vacancies of the $[Fe(CN)_6]$ sites would allow us to chemically tune the phase transition temperature. In order to test this, various FeCo Prussian blue analogues with different Co/Fe ratios were prepared using a simple solution reaction of $CoCl_2{\cdot}6H_2O$ and $Na_3[Fe(CN)_6]$ by controlling the NaCl concentration and temperature.[16] The resulting formulas and the valence states of the synthesized compounds **2c**–**2g** are listed in Table 2. The $\chi_M T$ vs T plots are shown in Fig. 25. The figures clearly show that the phase transition temperature strongly depends on the Co/Fe ratio. That is, the larger the Co/Fe ratio, the lower the spin transition temperature. This means that, in fact, the phase transition temperature can be controlled by a chemical method. It should be noted that Escax et al.[103] and Goujon et al.[104] have also reported the control of the thermally induced electron transfer by the $[Fe^{III}(CN)_6]$ vacancies in similar compounds: $Cs_xCo^{II\text{-}HS}{}_4$-$[Fe^{III}(CN)_6]_y$.

Let us mention the photo-magnetism of these compounds. It was found that compounds **2c**–**2f** show a photo-induced magnetization. As was seen in Fig. 26, the relaxation temperatures tend to decrease with a smaller Co/Fe ratio: 145 K (**2d**); 125 K (**2e**); 110 K (**2f**). This observation means that the larger free energy difference (ΔG_0) at low temperature produces a smaller activation energy (ΔG^*). This relationship is explained by the conventional energy gap dependence of the electron-transfer reaction in the normal region.[105] Calculation of the potential energy surfaces for the FeCo Prussian blue analogues show that a compound with a lower defect site has a larger ΔG_0 value but a smaller ΔG^* value.[101]

Table 2. Formula and Valence State of Compounds **2c**–**2g**

Compound	Formula	Valence state at 290 K
2c	$Na_{0.07}Co_{1.50}Fe(CN)_6{\cdot}6.3H_2O$	$Na_{0.07}Co^{II}{}_{1.50}[Fe^{III}(CN)_6]_{0.93}[Fe^{II}(CN)_6]_{0.07}{\cdot}6.3H_2O$
2d	$Na_{0.37}Co_{1.37}Fe(CN)_6{\cdot}4.8H_2O$	$Na_{0.37}Co^{II}{}_{1.37}[Fe^{III}(CN)_6]_{0.89}[Fe^{II}(CN)_6]_{0.11}{\cdot}4.8H_2O$
2e	$Na_{0.53}Co_{1.32}Fe(CN)_6{\cdot}4.4H_2O$	$Na_{0.53}Co^{II}{}_{1.32}[Fe^{III}(CN)_6]_{0.83}[Fe^{II}(CN)_6]_{0.17}{\cdot}4.4H_2O$
2f	$Na_{0.60}Co_{1.26}Fe(CN)_6{\cdot}3.9H_2O$	$Na_{0.60}Co^{III}{}_{0.18}Co^{II}{}_{1.08}[Fe^{III}(CN)_6]_{0.70}[Fe^{II}(CN)_6]_{0.30}{\cdot}3.9H_2O$
2g	$Na_{0.94}Co_{1.15}Fe(CN)_6{\cdot}3.0H_2O$	$Na_{0.94}Co^{III}{}_{0.76}Co^{II}{}_{0.39}[Fe^{II}(CN)_6]{\cdot}3.0H_2O$

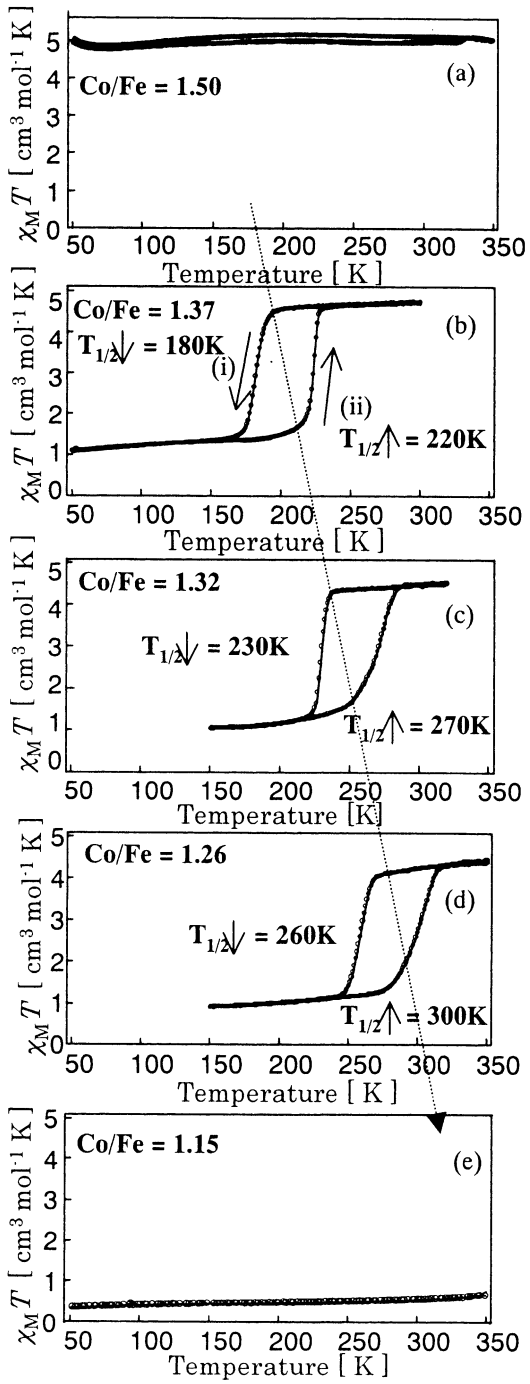

Fig. 25. Temperature dependence of the magnetization of compounds (a) **2c**, (b) **2d**, (c) **2e**, (d) **2f**, and (e) **2g**. The phase transitions of the **2d–2f** are accompanied by a large thermal hysteresis. The transition temperatures for **2d–2f** are $T_{1/2}\downarrow$ = 180 K and $T_{1/2}\uparrow$ = 220 K ($\Delta T = T_{1/2}\uparrow - T_{1/2}\downarrow$ = 40 K), $T_{1/2}\downarrow$ = 230 K and $T_{1/2}\uparrow$ = 270 K (ΔT = 40 K) and $T_{1/2}\downarrow$ = 260 K and $T_{1/2}\uparrow$ = 300 K (ΔT = 40 K), respectively.[16]

3. Photo-Induced Valence Tautomerism in a Co Compound[19–24]

Valence tautomerism is characterized by the different species having different distributions of electron density, where

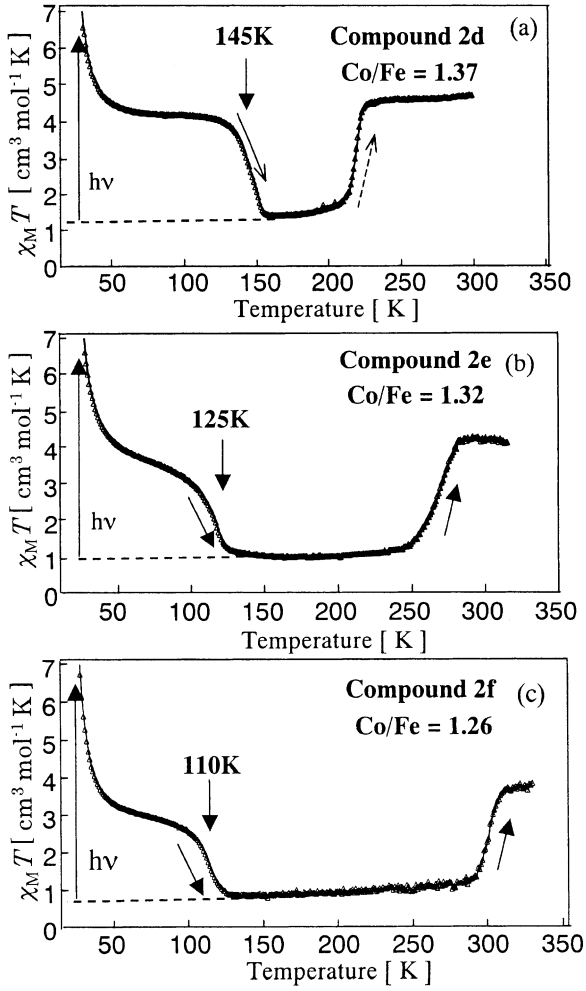

Fig. 26. $\chi_M T$ versus T plots for the photo-irradiated compounds (a) **2d**, (b) **2e**, and (c) **2f**. After the photoirradiation was finished, the measurements of susceptibility during the warming process were performed in the dark at H = 5000 G.

metal-to-ligand electron transfer accomplishes interconversion between tautomers.[106–111] Buchanan et al. reported that a Co complex, $[Co^{II\text{-}HS}(3,5\text{-dbsq})_2(bpy)]$ (bpy = 2,2′-bipyridine), shows Co-quinone electron transfer in a toluene solution.[106] The intra-molecular charge transfer process can be expressed as

$$[Co^{II\text{-}HS}(3,5\text{-dbsq})_2(bpy)] \leftrightarrows [Co^{III\text{-}LS}(3,5\text{-dbsq})(3,5\text{-dbcat})(bpy)].$$

Similar intra-molecular charge transfer has been observed in solid-state Co complexes.[80,112] Furthermore, it has been reported that charge transfer can be induced by visible light as well as by changes in temperature.[113,114] Unfortunately, thermal back-transfer of electrons proceeds at an appreciable rate in these systems, limiting their use in practical applications. Here, we describe how the Co compounds, $[Co^{III\text{-}LS}(3,5\text{-dbsq})(3,5\text{-dbcat})(phen)]\cdot C_6H_5CH_3$ (**3a**),[19–21] $[Co^{III\text{-}LS}(3,5\text{-dbsq})(3,5\text{-dbcat})(tmeda)]\cdot 0.5C_6H_5CH_3$ (**3b**),[22,23] and $[Co^{III\text{-}LS}(3,6\text{-dbsq})(3,6\text{-dbcat})(tmpda)]$ (**3c**),[24] where phen, tmeda and tmpda are

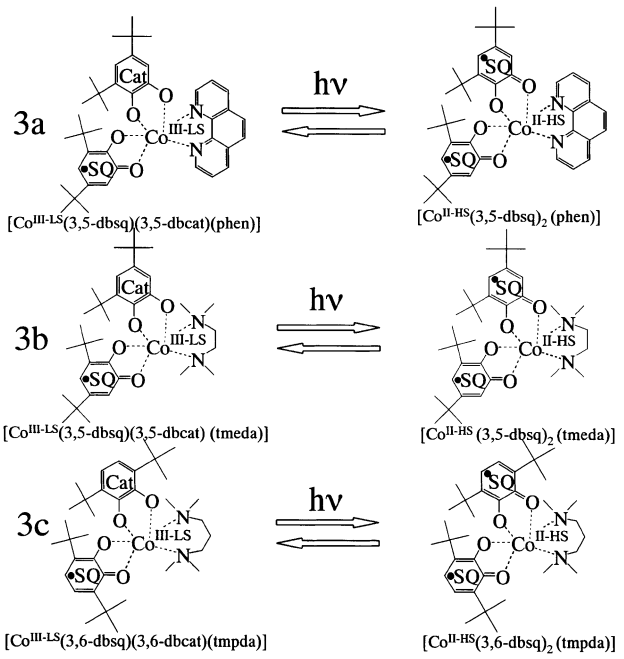

Fig. 27. Photoinduced valence tautomerism in Co complexes, **3a** (top), **3b** (middle) and **3c** (bottom). The Co complexes **3a** and **3c** were prepared as previously described.[80,112,116,117] The Co complex, **3b**, was prepared by adding 15mL of a solution of tmeda (0.046 g) in toluene to 50mL of a solution of $[Co(3,5\text{-dbsq})_2]_4$ (0.20 g) suspended in toluene, followed by slow evaporation under flowing Ar gas.

1,10-phenanthrolin, *N*,*N*,*N*′,*N*′-tetramethylethylenediamine and *N*,*N*,*N*′,*N*′-tetramethylpropylenediamine respectively, show a long-lived intra-molecular charge transfer in response to visible light (Fig. 27). It should be noted that compounds, **3a** and **3c**, have been synthesized by Adams et al.[80,112,114,115] and Jung et al.[116] respectively, and that their basic physical properties have been extensively studied by the same groups.

3-1. Valence Tautomerism of Co Complexes. The crystal structures of compounds **3a** and **3c** have been reported by Adams et al.[80] and Jung et al.,[117] respectively. The space group for each of them is monoclinic ($P2_1/c$). The X-ray structure of **3b**, measured by us, is shown in Fig. 28.[23]

The μ_{eff} versus T curves, where μ_{eff} is the molar effective magnetic moment and T is the temperature, are shown in Fig. 29. The compounds **3a**, **3b** and **3c** exhibit valence tautomerism at around 240 K, 195 K and 165 K, respectively. Their valence tautomeric behaviour

$[Co^{\text{II-HS}}(3,5\text{-dbsq})_2(\text{phen})]$
$\leftrightarrows [Co^{\text{III-LS}}(3,5\text{-dbsq})(3,5\text{-dbcat})(\text{phen})]$,
$[Co^{\text{II-HS}}(3,5\text{-dbsq})_2(\text{tmeda})]$
$\leftrightarrows [Co^{\text{III-LS}}(3,5\text{-dbsq})(3,5\text{-dbcat})(\text{tmeda})]$,
$[Co^{\text{II-HS}}(3,6\text{-dbsq})_2(\text{tmpda})]$
$\leftrightarrows [Co^{\text{III-LS}}(3,6\text{-dbsq})(3,6\text{-dbcat})(\text{tmpda})]$,

is consistent with that reported previously.[80,112,116,117] A phase transition accompanies the colour change from dark green-brown at room temperature to blue-black at low temperature. Figure 30 shows the change in the absorption spectra. The

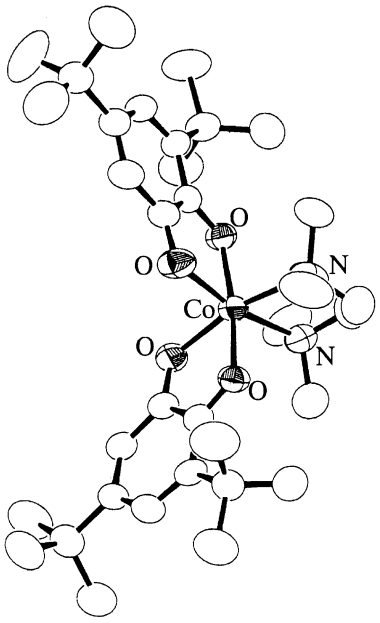

Fig. 28. View of $[Co^{\text{II-HS}}(3,5\text{-dbsq})_2(\text{tmeda})]$ (**3b**). The crystallographic properties are as follows: Fw = 1323.66, green needle-like crystal (0.5×0.1×0.1), triclinic, space group $P\bar{1}$, a = 15.0805(5), b = 15.9615(2), c = 18.4550(3) Å, α = 67.655(2), β = 75.268(2), γ = 73.783(3)°, V = 3890.0(2) Å^3, Z = 2, D_{calcd} = 1.130 g cm^{-3}.[23]

characteristic absorption band of the high-temperature phase is the $Co^{\text{II-HS}}$ to dbsq (dbsq = 3,5-dbsq and 3,6-dbsq) charge transfer (CT) band observed at around 750–800 nm. On the other hand, the low temperature phase has an absorption band at around 600 nm, which is characteristic of a ligand field in nature, but it does contain some charge transfer from dbcat (dbcat = 3,5-dbcat and 3,6-dbcat) to $Co^{\text{III-LS}}$. Additionally, in the near-IR region, the phase has a CT band from dbcat to dbsq at around 2500 nm.[115]

3-2. Photo-Induced Valence Tautomerism. In order to excite the dbcat to $Co^{\text{III-LS}}$ CT band, the complexes were illuminated in the cavity of a SQUID with 532 nm light from a diode pumped Nd:YAG laser. As shown in Fig. 29, the magnetization value increased after illumination. This indicates that the following intra-molecular electron transfer from dbcat to $Co^{\text{III-LS}}$ is induced by the illumination:

$[Co^{\text{III-LS}}(3,5\text{-dbsq})(3,5\text{-dbcat})(\text{phen})]$
$\rightarrow [Co^{\text{II-HS}}(3,5\text{-dbsq})_2(\text{phen})]$,
$[Co^{\text{III-LS}}(3,5\text{-dbsq})(3,5\text{-dbcat})(\text{tmeda})]$
$\rightarrow [Co^{\text{II-HS}}(3,5\text{-dbsq})_2(\text{tmeda})]$,
$[Co^{\text{III-LS}}(3,6\text{-dbsq})(3,6\text{-dbcat})(\text{tmpda})]$
$\rightarrow [Co^{\text{II-HS}}(3,6\text{-dbsq})_2(\text{tmpda})]$.

The magnetisation values at 5 K after illumination are ca. 2.8, 2.3 and 2.03 μ_B (Bohr Magneton) for **3a**, **3b** and **3c**, respectively. The small magnetization value (2.03–2.8 μ_B) compared with the value at 300 K (5.1–5.2 μ_B) can be explained by the presence of an antiferromagnetic interaction between $Co^{\text{II-HS}}$ and 3,5-dbsq (see Section 3–5), and by the overlap of the 3,5-dbcat to $Co^{\text{III-LS}}$ absorption and the $Co^{\text{II-HS}}$ to 3,5-dbsq absorp-

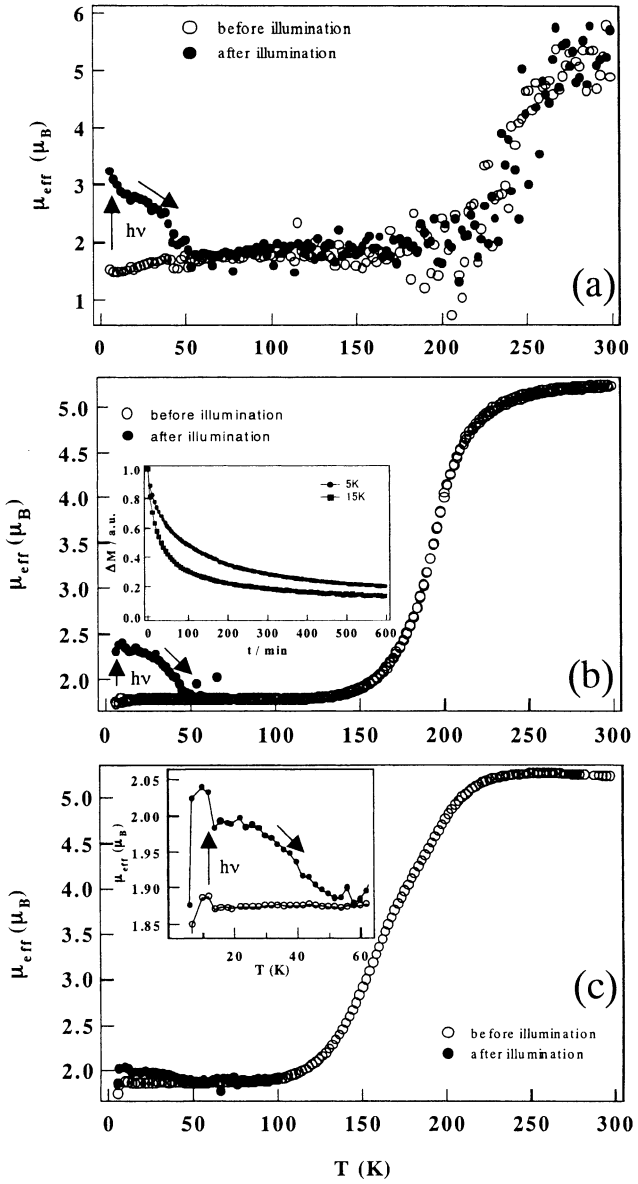

Fig. 29. The μ_{eff} versus T plots before (○) and after (●) illumination at 5 K for compounds **3a** (top), **3b** (middle) and **3c** (bottom).[20, 22, 24] The sweep rate is 2 K min^{-1}. The μ_{eff} values for **3a**, **3b** and **3c** at 300 K are equal to 5.1, 5.2 and 5.2 μ_B, respectively. On the other hand, their μ_{eff} values at 5 K are equal to 1.7, 1.7 and 1.87 μ_B, respectively. After the excitation of the LMCT band, the magnetization value increased to 2.8 μ_B (**3a**), 2.3 μ_B (**3b**) and 2.03 μ_B (**3c**) at 5 K. Inset of (b): Relaxation curves after illumination at 5 K and 15 K of **3b**. If the lifetime is defined as the time when the magnetisation is reduced to 1/e of the initial change induced by the light, the lifetimes at 5 and 15 K are 175 and 70 min, respectively. Note that the lifetimes at 5, 15 and 35 K for **3a** and that at 5 K for **3c** are 96, 47, 11 and 15 min, respectively. Inset of (c): expanded plots from 0 to 60 K. The notation *hν* represents illumination at 5 K.

tion (see Section 3–7). The μ_{eff} versus T curve measured at a rate of 2 K min^{-1} after illumination in the heating mode shows that the metastable state recovered to the original state at around 50 K. This means that the lifetime at 50 K becomes less than several seconds, which is the time window of our SQUID system.

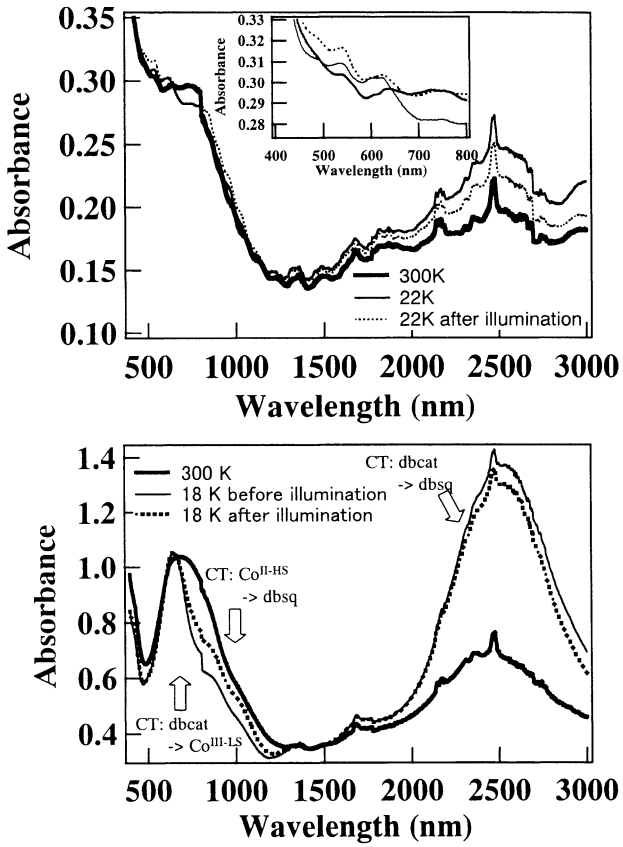

Fig. 30. (Top) UV-vis spectra of **3a** at 300 K and 22 K before and after illumination.[20] Inset: expanded spectra from 400 to 800 nm. (Bottom) UV-vis spectra of **3b** at 300 K, 18 K before and after illumination.[22]

The absorption spectra of **3a** before and after illumination are shown in Fig. 30. The Co^{II-HS} to 3,5-dbsq CT band at around 750 nm, characteristic of the [Co^{II-HS}(3,5-dbsq)$_2$(phen)] state, is significantly increased. It is found that the absorption spectra after illumination resembles the spectra measured at room temperature. Figure 30 also shows the near-IR spectra before and after illumination. The absorption band at 2500 nm, which is ascribable to the CT from 3,5-dbcat to 3,5-dbsq of the [Co^{III-LS}(3,5-dbsq)(3,5-dbcat)(phen)] state, is reduced after illumination. These spectra show that the CT from 3,5-dbcat to Co^{III-LS} is induced by light. Similar changes could be observed for **3b** and **3c**.

3-3. Photo-Induced Change in IR, UV-Vis and EPR Spectra. The IR spectrum of the Co complex was measured in order to confirm the electronic state of the metastable form. The C–O stretching modes are sensitive to the charge of the ligand moieties. The C=O stretch for free quinone was observed at around 1675 cm^{-1}. On the other hand, the peak shifts to lower energy by ca. 60 cm^{-1} when the quinone is coordinated to a metal ion.[118] Furthermore, when the quinone is reduced to dbsq and dbcat, the stretching mode shifts further to lower frequency. Figure 31 shows that the C–O stretch vibration of dbcat in [Co^{III-LS}(dbsq)(dbcat)(NN)] (NN = phen, tme-

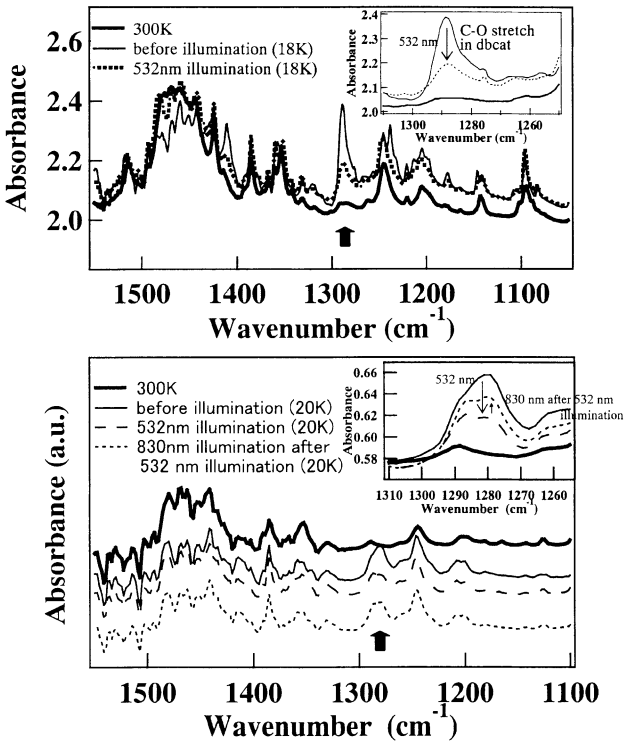

Fig. 31. IR spectra before and after illumination of **3a** (top) and **3b** (bottom).[20,22] Inset: expanded spectra from 1310 to 1255 cm^{-1}. The C–O stretch peak is reduced by the excitation of the LMCT band with 532 nm light, because they convert to the metastable state, [$Co^{II\text{-}HS}$(3,5-dbsq)$_2$(NN)]. On the other hand, the C–O stretch peak of **3b**, which is reduced by the excitation of the LMCT band, is clearly increased after the excitation of the MLCT band with 830 nm light. This means that the 830nm light induced the reverse valence tautomerism.[23]

da and tmpda) is observed at 1288, 1280 and 1279 cm^{-1} for **3a**, **3b** and **3c**, respectively. On warming, the peak decreased significantly. This is because dbcat is oxidized to dbsq via thermally-induced valence tautomerism. When the complex, [$Co^{III\text{-}LS}$(dbsq)(dbcat)(NN)], is illuminated at low temperature, the peak at around 1280 cm^{-1} is significantly decreased. This is consistent with the proposal that visible light induces charge transfer from dbcat to $Co^{III\text{-}LS}$. When the fraction of the metastable state was estimated from the IR peaks at around 1280 cm^{-1}, it was found that about 70 ± 10% (**3a**), 50 ± 10% (**3b**) and 10 ± 5% (**3c**) of the moieties were changed from [$Co^{III\text{-}LS}$-(dbsq)(dbcat)(NN)] to [$Co^{II\text{-}HS}$(dbsq)$_2$(NN)] by illumination. Note that these values are larger than those estimated from UV-vis spectra. This discrepancy might arise from the different sampling conditions for the two measurements; the IR measurements were performed by the KBr method, while the UV-vis spectra were measured for a polystyrene film in which the Co complex was embedded. It is thought that the Co complexes are dispersed randomly in the polystyrene film and hence no cooperative interaction operates. If this is the case, the cooperativity due to the intermolecular interaction is essential to achieving photoinduced valence tautomerism. Further study to clarify this problem is in progress.

The X-band EPR spectra also support the occurrence of

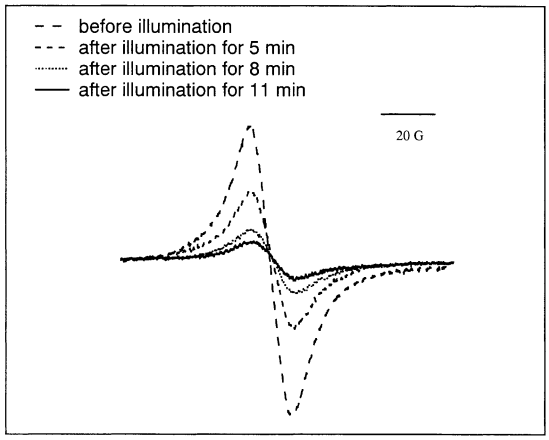

Fig. 32. ESR spectra before and after illumination of **3a** at 6 K.

photoinduced valence tautomerism (Fig. 32). The $Co^{III\text{-}LS}$ complexes with 3,5-dbsq and 3,5-dbcat ligands in a frozen glass typically show a signal centred at g = ca. 2, with eight hyperfine lines due to coupling to the ^{59}Co (I = 7/2) nucleus,[106] while, as powder samples, they do not show the hyperfine coupling with ^{59}Co (I = 7/2).[119] Furthermore, it has been reported that the EPR signal is significantly reduced when the $Co^{III\text{-}LS}$ complexes changed to the $Co^{II\text{-}HS}$ state with two 3,5-dbsq ligands.[106] Figure 32 shows the EPR spectra of **3a** measured at 6 K. It exhibits a signal with g values close to 2.00, showing the presence of a one ligand-based radical species. This is consistent with the fact that the Co complex, **3a**, has the electronic state of [$Co^{III\text{-}LS}$(3,5-dbsq)(3,5-dbcat)(phen)] at 6 K. The absence of the hyperfine coupling with ^{59}Co (I = 7/2) also agrees with the previous report described above. When the [$Co^{III\text{-}LS}$-(3,5-dbsq)(3,5-dbcat)(phen)] complex was illuminated at 6 K, the EPR signal was significantly reduced. This change is consistent with the induction of the electron transfer from 3,5-dbcat to $Co^{III\text{-}LS}$.

3-4. XANES and EXAFS Measurement.[21] It is important to note that there is another possible explanation for the photo-induced change in the magnetization. That is, the photo-induced metastable state may have an electronic state of [$Co^{II\text{-}LS}$-(dbsq)$_2$(NN)], not [$Co^{II\text{-}HS}$(dbsq)$_2$(NN)]. In order to identify the electronic state and local structure around the Co in the metastable state, XANES and EXAFS spectra were measured. Figure 33 shows the Co K-edge XANES spectra of **3a**. The spectra measured at 30 and 300 K are consistent with those reported previously.[120] The energy shift originates from the drastic electronic and structural changes around the Co due to thermally induced valence tautomerism. The energy separation of the first intense resonance between 30 and 300 K is around 4 eV, which is in good agreement with that of the FeCo Prussian blue described above.[17,18]

When complex **3a** is illuminated with visible light (532 nm) at 11 K, a large change in the spectra was observed. As shown in the Figure, the spectrum looks like a superposition of the spectrum measured at 30 K and the spectrum at 300 K, i.e. a superposition of the spectra of the high temperature phase and of the low temperature phase. In fact, the spectrum after illumination could be simulated by summing 65% of the 300 K

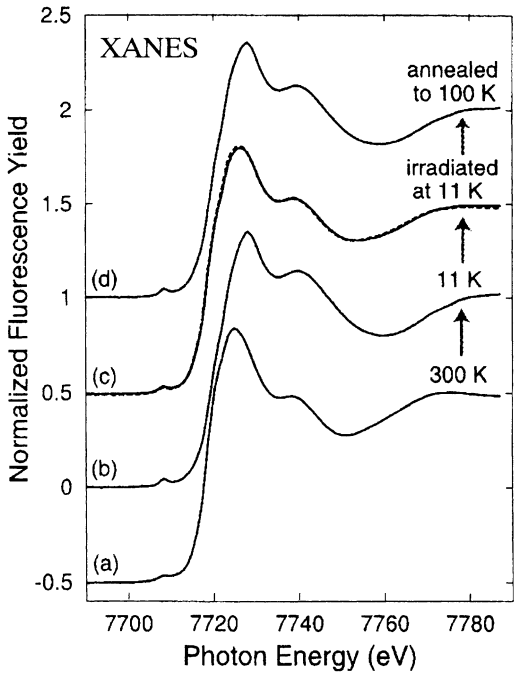

Fig. 33. Co *K*-edge XANES spectra taken with the fluorescence-yield mode: (a) 300 K; (b) 11 K; (c) during visible-light illumination (solid line), together with the simulated spectrum obtained by the superposition of the 300 K and 11 K spectra with a ratio of 0.65:0.35 (dashed line); (d) after annealing to 100 K for the illuminated sample.[21]

spectrum and 35% of the 30 K spectrum. The fact that 65% of the moieties changed to the metastable state is consistent with the value (70%) estimated from the IR spectra. Thus, it is concluded that the photo-induced trapped excited state is essentially identical to the high temperature phase. Furthermore, the spectrum of the $Co^{II\text{-}LS}$ state should be noticeably different to that of the $Co^{II\text{-}HS}$, as is found in some Co^{II} spin-crossover complexes.[121] This also excludes the possibility of $Co^{II\text{-}LS}$ for the photoinduced metastable state. The changed XANES spectra could be reverted to the original state by heating the sample above 50 K, showing that the relaxation involving the electron transfer from $Co^{II\text{-}HS}$ to 3,5-dbsq is thermally induced.

3-5. Presence of Anti-Ferromagnetic Interaction. An important characteristic of the photo-effects described here is that the magnetisation value after illumination does not reach the level observed for $[Co^{II\text{-}HS}(3,5\text{-dbsq})_2(NN)]$ at 300 K. In the case of **3b**, the experimental value at 5 K after illumination is 2.3 μ_B. On the other hand, at a first glance, the magnetisation value should be 3.5 μ_B, assuming that 50% of the moieties change to the $[Co^{II\text{-}HS}(3,5\text{-DBSQ})_2(tmeda)]$ state with 5.1 μ_B at 300 K. In our opinion, such a small magnetisation value can be explained by the presence of intramolecular magnetic exchange interactions between the dbsq ligands and the $Co^{II\text{-}HS}$ ion. In fact, the magnetic interaction of $[Co^{II\text{-}HS}{}_4(3,5\text{-dbsq})_8]$ is anti-ferromagnetic, with an exchange parameter of $J = -30$ cm^{-1}.[122] Furthermore, it has been reported that the interaction in $[Co^{II\text{-}HS}(3,5\text{-dbsq})_2(phen)]$ can be calculated to be anti-ferromagnetic in nature with $J = -594$ cm^{-1}.[115] As in the case of those compounds, anti-ferromagnetic interactions are expected between dbsq and the $Co^{II\text{-}HS}$ ion for $[Co^{II\text{-}HS}(dbsq)_2(NN)]$ as

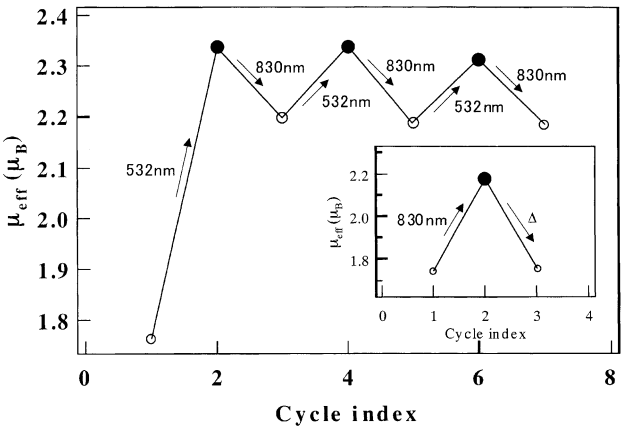

Fig. 34. Change in the magnetization by alternate illumination with 532 nm light and with 830 nm light. Inset: Change in the magnetization induced by illumination with 830 nm light and by thermal treatment (△) at 60 K.[23]

follows. The exchange interactions in the compounds under consideration here can be divided into two types. The interaction between the π orbital of dbsq and the e_g orbital of the $Co^{II\text{-}HS}$ is ferromagnetic, because they are orthogonal to each other. The other interaction between the π orbital of dbsq and the t_{2g} orbital of the $Co^{II\text{-}HS}$ gives rise to anti-ferromagnetic character because they overlap with each other. When the ferromagnetic and anti-ferromagnetic interactions are superimposed, the anti-ferromagnetic term, in general, dominates the interactions. The presence of the anti-ferromagnetic exchange interactions gives rise to four different electronic states: one $S = 1/2$ spin state with the lowest energy, two $S = 3/2$ states and one $S = 5/2$ state with the highest energy. Hence, the $S = 1/2$ state is mainly populated at sufficiently low temperatures due to the Boltzmann distribution. As a result, the magnetisation value after illumination is small compared with that in the high temperature phase.

3-6. Photo-Induced Reverse Valence Tautomerism. The metastable states of **3a**, **3b** and **3c**, $[Co^{II\text{-}HS}(dbsq)_2(NN)]$, have a charge transfer (CT) band from $Co^{II\text{-}HS}$ to dbsq at around 750–800 nm. Hence, it might be possible to convert the metastable state back to the ground state by selectively illuminating the metal-to-ligand charge transfer (MLCT) band. In fact, when back electron transfer was investigated for **3b** and **3c**, we found that the metastable states revert to the original ones via reverse electron transfer.

The photoinduced change in the magnetization of **3b** was shown in Fig. 34. The magnetization value was ca. 2.3 μ_B before the excitation of the MLCT band. When the metastable complex, $[Co^{II\text{-}HS}(3,5\text{-dbsq})_2(tmeda)]\cdot 0.5C_6H_5CH_3$, was illuminated with 830 nm light (ca. 30 mW/cm^2), the magnetization value decreased. As shown in the figure, the magnetization value after excitation of the MLCT band is ca. 2.2 μ_B. This means that the back electron transfer from the $Co^{II\text{-}HS}$ to the 3,5-DBSQ was induced by light. The photo-process can be expressed as

$[Co^{II\text{-}HS}(3,5\text{-dbsq})_2(tmeda)]\cdot 0.5C_6H_5CH_3$ (metastable state)
$\rightarrow [Co^{III\text{-}LS}(3,5\text{-dbsq})(3,5\text{-dbcat})(tmeda)]\cdot 0.5C_6H_5CH_3$
(ground state)

The induction of the back electron transfer was confirmed by the UV-vis and the IR spectra. Figure 31 shows the IR spectra measured before and after illumination with 830 nm light.

Additionally, it was found that alternate illumination with 532 nm and with 830 nm light can induce a reversible change in magnetization, as shown in Fig. 34.

3-7. Achievement of a Photo-Stationary State. It should be noted that the magnetization value does not reach the original level observed for the pure [$Co^{III\text{-}LS}$(dbsq)(dbcat)(NN)] state at 5 K, i.e. ca. 1.7 μ_B. As is described above, the magnetization value of [$Co^{II\text{-}HS}$(3,5-dbsq)$_2$(tmeda)] decreased from ca. 2.3 to 2.2 μ_B due to 830 nm light illumination. This suggests that 70% of the moieties, whose electronic state was changed from [$Co^{III\text{-}LS}$(3,5-dbsq)(3,5-dbcat)(tmeda)] to [$Co^{II\text{-}HS}$(3,5-dbsq)$_2$(tmeda)] by 532 nm light, remain unchanged after illumination with 830 nm light. This suggests that the magnetization value, μ_{eff} = ca. 2.2 μ_B, is observed as a result of the achievement of the photo-stationary state under the illumination with 830 nm light. That is, the excitation at a wavelength of 830 nm induces both the LMCT in the [$Co^{III\text{-}LS}$(3,5-dbsq)(3,5-dbcat)(tmeda)] (ground state) as well as MLCT in the [$Co^{II\text{-}HS}$(3,5-dbsq)$_2$(tmeda)] (metastable state). In fact, the edge of the LMCT band extends toward a wavelength of 830 nm. This is consistent with the observation that, when the complex with the electronic state [$Co^{III\text{-}LS}$(3,5-dbsq)(3,5-dbcat)(tmeda)]·0.5$C_6H_5CH_3$ was illuminated with 830 nm light at 5 K, an increase in the magnetization value from ca. 1.7 to 2.2 μ_B was observed (Fig. 34). The achievement of a photo-stationary state was also confirmed by an investigation of the wavelength dependence of the photo-effects.[22]

3-8. Photo-Induced Charge Transfer Process. The charge transfer process is illustrated schematically in Fig. 35. The spin-allowed transition, [$Co^{III\text{-}LS}$(dbsq)(dbcat)(NN)] → [$Co^{II\text{-}LS}$(dbsq)$_2$(NN)], is induced by exciting the CT band from dbcat to $Co^{III\text{-}LS}$. After excitation, some fractions of the excited state relax back to the initial state. However, an alternative spin forbidden decay path, [$Co^{II\text{-}LS}$(dbsq)$_2$(NN)] → [$Co^{II\text{-}HS}$-(dbsq)$_2$(NN)], could be possible due to spin-orbit coupling. Consequently, the metastable [$Co^{II\text{-}HS}$(dbsq)$_2$(NN)] state can be populated by using visible light. Note that the direct transition from [$Co^{III\text{-}LS}$(dbsq)(dbcat)(NN)] to [$Co^{II\text{-}HS}$(dbsq)$_2$(NN)] is spin forbidden, and hence the process cannot be seen in the spectrum. In a similar manner, back electron transfer could be induced by exciting the MLCT band.

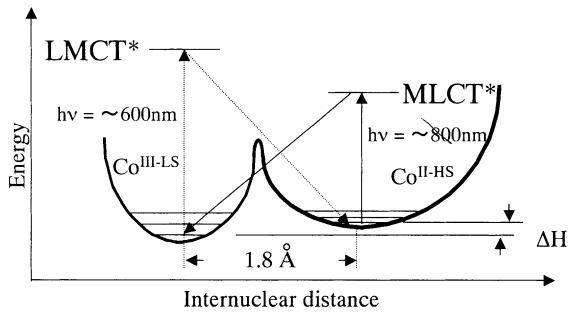

[$Co^{III\text{-}LS}$(3,5-dbsq)(3,5-dbcat)(phen)] [$Co^{II\text{-}HS}$(3,5-dbsq)$_2$(phen)]

[$Co^{III\text{-}LS}$(3,5-dbsq)(3,5-dbcat)(tmeda)] [$Co^{II\text{-}HS}$(3,5-dbsq)$_2$(tmeda)]

[$Co^{III\text{-}LS}$(3,6-dbsq)(3,6-dbcat)(tmpda)] [$Co^{II\text{-}HS}$(3,6-dbsq)$_2$(tmpda)]

Fig. 35. Simplified energy-level diagram.

The difference in energy between [$Co^{III\text{-}LS}$(3,5-dbsq)(3,5-dbcat)(phen)] and [$Co^{II\text{-}LS}$(3,5-dbsq)$_2$(phen)] has been estimated to be 0.278 eV,[114] meaning that 26.8 J can be stored per mole. The bottoms of the potential wells for [$Co^{III\text{-}LS}$(dbsq)-(dbcat)(NN)] and [$Co^{II\text{-}LS}$(dbsq)$_2$(NN)] were about 0.18 Å.[80] The Co *K*-edge EXAFS measurements reveal that the average Co–N,O distances for the high-temperature and low-temperature phases are 2.081 Å and 1.904 Å respectively. The difference, 0.177 Å, is consistent with the above value (0.18 Å). It is thought that the existence of two minima in the potential energy curves, with the [$Co^{III\text{-}LS}$(dbsq)(dbcat)(NN)] state being lower in energy than the [$Co^{II\text{-}LS}$(dbsq)$_2$(NN)] state, and the operation of cooperative interactions in the crystal have allowed the observation of the long-lived metastable state.

3-9. Relevance to Photomechanical Effects and Solar Energy Storage. It is important to note that photomechanical effects involving intramolecular charge transfer have been reported in several compounds.[123–126] That is, when crystals such as [Rh^{I}(3,6-dbsq)(CO)$_2$] and [$Co^{III\text{-}LS}$(3,6-dbsq)(3,6-dbcat)(pyrazine)] are illuminated, they bend reversibly in response to the light. However, these photomechanical effects can be effectively induced by the near-IR light from a tungsten-halogen lamp, which is different from the present phenomena.

Furthermore, it is interesting to compare the Co valence tautomeric compounds with the layered zirconium phosphonate/viologen compounds. Vermeulen et al. have reported the observation of long-lived charge separation in zirconium compounds.[127] Although this is quite an interesting system, the charge separation can only be induced by UV-light. Hence, it has been pointed out that the photo-response needs to be moved to longer wavelengths, i.e. the visible region.[128] By contrast, visible light can be used to induce charge transfer in the present Co complexes, so a larger fraction of the solar spectrum can be absorbed. This means that the present Co system will be important from the viewpoint of solar energy storage.

4. Optically Switchable Fe^{III} Spin Crossover Complex and Cu^{II} Thermochromic Compound.[25,26]

Here, we would like to briefly describe examples of photo-induced spin crossover in an Fe^{III} complex and photo-induced structural changes in a Cu^{II} complex that were recently discovered by our group.

4-1. First Observation of Light-Induced Excited Spin State Trapping in an Fe^{III} complex.[25] In 1984 Decurtines et al. reported a light-induced excited spin state trapping effect in an Fe^{II} complex.[129] Since the first observation of the LIESST effect, many LIESST complexes have been reported. However, only Fe^{II} complexes have so far shown the LIESST effect, and the observation of the LIESST effect in Fe^{III} and Co^{II} molecular solids was unexpected.[3] The reason for this is "the tunneling effect". Figure 36 shows the change in the ligand-to-metal bond length between the high-spin and low-spin states. In the high-spin state, the ligand-to-metal bond length is relatively long, because two electrons occupy the e_g orbital with an anti-bonding character. It has been reported that these differ-

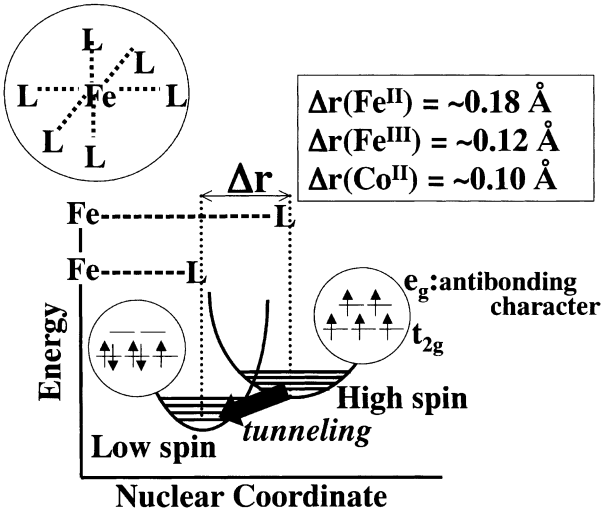

Fig. 36. Schematic illustration of the difference (Δr) in the metal to ligand bond length between high-spin and low-spin states. It has been reported that Δr for Fe^{II}, Fe^{III} and Co^{II} complexes are about 0.18, 0.12 and 0.10 Å, respectively.

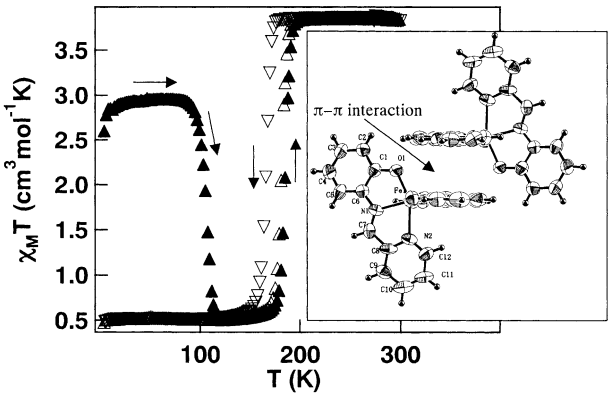

Fig. 37. $\chi_m T$ versus T plots for $[Fe(pap)_2]ClO_4 \cdot H_2O$. The sample was cooled from 300 K to 5 K (▽) and then warmed from 5 K to 300 K (△) at a rate of 2 K min^{-1}. The sample was warmed at a rate of 2 K min^{-1} after it had been quenched to 5 K (▲). Inset: structure of the π–π stacking between $[Fe(pap)_2]ClO_4 \cdot H_2O$ complexes.[25]

ences for Fe^{II}, Fe^{III} and Co^{II} are about 0.18, 0.12 and 0.10 Å, respectively. That is, the difference for Fe^{III} and Co^{II} is smaller than that for Fe^{II}. Hence, because of this small structural change, the meta-stable states of the Fe^{III} and Co^{II} complexes are easily restored to their original state due to the tunneling effects of the atoms. As a result, until now the general belief has been that Fe^{III} complexes can never show LIESST effects. However, this expectation was based on a model developed for isolated molecules, and molecular interactions were not taken into consideration. We think that if strong molecular interactions are introduced into molecular compounds, observation of the LIESST effect might be possible, even for Fe^{III} and Co^{II} compounds. This is because the cooperativity resulting from the molecular interaction operates to increase the activation energy, potentially preventing the relaxation by tunneling effect as well as the thermal relaxation at low temperature. Therefore, our strategy to achieve Fe^{III} LIESST effects is to introduce strong inter-molecular interactions by using π–π interactions, hydrogen bonding and coordinate bonding. Based on this strategy, we have focused on Fe^{III} complexes with planar tridentate ligands. This is because, in general, those molecules with planar ligands tend to stick to each other by strong π–π interactions. In fact, their crystal structure shows that Fe^{III} molecules with planar tridentate ligands, such as $[Fe^{III}(pap)_2]$-$ClO_4 \cdot H_2O$,[130] are connected to each other by the π–π interactions of their ligands (Fig. 37). This suggests that cooperative interactions might operate within the crystal, as we expected. The presence of the strong molecular interaction can be deduced experimentally from the magnetic properties of the complex (Fig. 37). On cooling, the magnetization value suddenly decreases at about 165 K and reaches 0.5 cm^3 mol^{-1} K. On warming, the magnetization increases abruptly at around 180 K. Furthermore, it was found that this complex exhibits a frozen-in effect. The abrupt spin transition and the frozen-in effect can be observed only when the cooperativity due to the π–π interaction is strong enough, suggesting that the rate of relaxation from the photoinduced metastable state in the Fe^{III} complex becomes quite slow.

In order to test this hypothesis, the effects of illumination on the Fe^{III} complex were investigated. It has been reported that a broad band observed around the visible region for the LS Fe^{III} complex can be attributed to the spin-allowed LMCT transition.[30] Furthermore, Schenker et al. reported that the excitation of the LMCT band results in the transient generation of high-spin Fe^{III} fractions.[30,131] Hence, in order to excite the LMCT band, we chose to use light with a wavelength of 400–600 nm that had been passed through an IR cut filter and a green filter. Figure 38 show a series of Mössbauer spectra that were recorded at 13 K before and after excitation with light. The spectrum measured before illumination at 13 K reveals a wide quadrupole-split doublet (I.S. = 0.11 mm s^{-1}, Q.S. = 3.08 mm s^{-1}), representing the low-spin state. The spectrum measured after illumination for 15 min shows a narrow quadrupole-split doublet (I.S. = 0.44 mm s^{-1}, Q.S. = 1.14 mm s^{-1}), representing the high-spin state. This means that the low-spin moieties were changed to the high-spin state by illumination. In analogy to a previous work, it is thought that illuminating the Fe^{III} complex with visible light induces the LMCT, followed by relaxation to the high-spin state. According to the Tanabe–Sugano diagram, the $^4T_1$ state is an intermediate state for the Fe^{III} LIESST process. When the temperature is raised to 150 K for a few minutes and then lowered again to 13 K, the metastable state was found to relax back to the low-spin ground state (I.S. = 0.11 mm s^{-1}, Q.S. = 3.08 mm s^{-1}). The metastable state could be maintained for a long time, provided that the sample was kept below ca. 70 K. The achievement of the anomalous long-lived metastable state is considered to be due to the presence of the strong inter-molecular interaction, because, as described above, the Fe^{III} complex is a conventional compound at the single molecule level. We believe our approach is valuable for developing novel optically switchable molecular compounds.

4-2. Light-Induced Structural Change in a Thermochromic Cu^{II} Complex.[26] The change in color of a transition

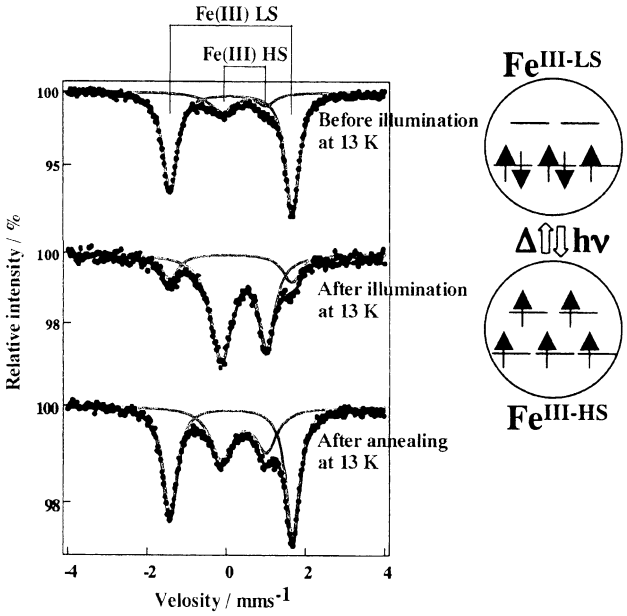

Fig. 38. ^{57}Fe Mössbauer spectra for $[Fe(pap)_2]ClO_4 \cdot H_2O$ at 13 K. (top) Spectrum before illumination. (middle) Spectrum after illumination. (bottom) Spectrum after thermal treatment at 130 K.[25]

metal complex under thermal excitation has recently evoked a lot of interest.[1,132] Solid state thermochromism can be divided into two categories; discontinuous thermochromism, where the color change takes place suddenly and is associated with a first order structural phase transition, and continuous thermochromism, where the color change is due to a gradual shift and broadening of the visible absorption upon stress with an increased population of the ground state vibrational levels. A typical example of such a discontinuous thermochromic compound is $[Cu^{II}(dieten)_2](BF_4)_2$.[133–141] The presence of the discontinuous character suggests that the Cu^{II} compound has bistable states, which are separated by a potential barrier in free energy. This means that the Cu^{II} compound potentially has the ability to exhibit photo-switching properties. In fact, we have discovered that the complex does exhibit a photo-induced long lived metastable state.

The Cu^{II} complex, $[Cu^{II}(dieten)_2](BF_4)_2$, was prepared by the method reported earlier.[133,134] When UV-light (250–400 nm) passed through a band-pass filter was used to illuminate the sample, a change in the color was observed. As shown in Fig. 39, the absorption peak at 455 nm, which is ascribable to the d–d transition of the Cu^{II} ion,[135] shifted to longer wavelength in the UV spectra. The magnetic properties measured at 5 K showed that no change was observed in the μ_{eff} value (1.8 μ_B) after UV light illumination. These results mean that the change is not due to redox isomerism, but to a change in the configuration of the complex. By analogy to previous work, the red shift in the d–d transition suggests that the square-planar configuration suffers a slight tetrahedral distortion due to the UV-light illumination (Fig. 39),[134,136,142,143] although further study to confirm this idea is needed.

The XRD patterns measured before and after illumination show that the photo-induced metastable state is different from that of the high-temperature phase. This means that transformation via a photo-process allows us to create a new phase, which is different from the thermally induced high-temperature phase. Because dynamic distortion should be substantially prevented at low temperature, it is thought that the structure of the metastable state has a static configuration, not a dynamic one.

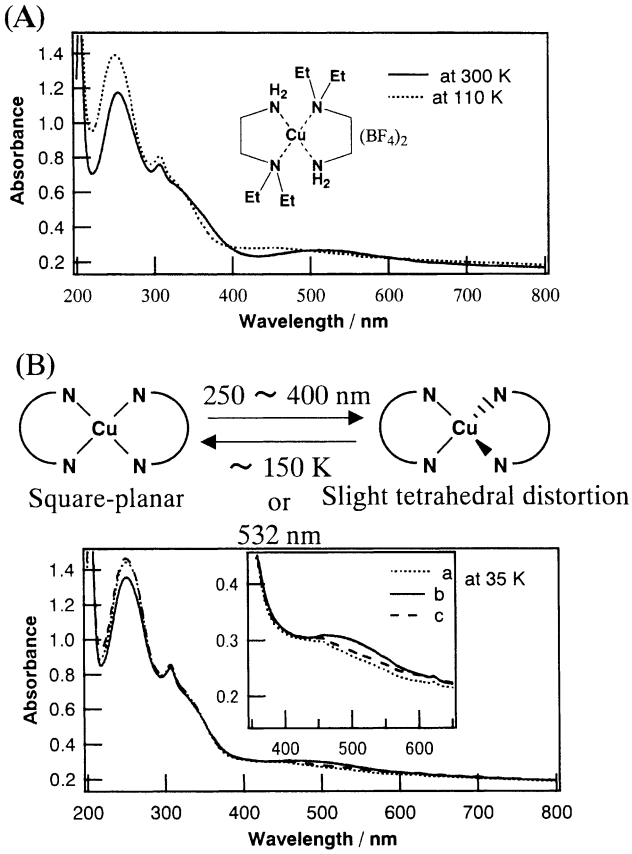

Fig. 39. (A) Temperature dependent absorption spectra and chemical structure of $[Cu(dieten)_2](BF_4)_2$. (B) Top: schematic illustration of the photoinduced structural change in $[Cu(dieten)_2](BF_4)_2$. Bottom: spectra (a) before and (b) after illumination, and (c) after thermal treatment to 150 K. Inset: expanded spectra from 350 to 650 nm.[26]

A similar photoinduced long-lived metastable state was observed for an analogous compound, $[Cu^{II}(dieten)_2](ClO_4)_2$.[133] We believe that materials that exhibit such bistability and strong cooperative interactions could often realize a photoinduced transformation.

5. Recent Advancements of Photoinduced Magnetization

Recently, many interesting photo-magnetic properties have been reported.[29,144–190] Here, we will introduce some examples of these (Table 3).

One recent advance in this field is the observation of photo-induced magnetization in an organic-based magnet. Nagai et al. reported a photo-induced spin-flopping phenomena in a charge transfer salt, MnTPP·TCNE.[145] On the other hand, Pejakovic et al. reported a photoinduced change in the magnetization for $Mn(TCNE)_x \cdot y(CH_2Cl_2)$.[146] These magnets are the first examples of reversible photoinduced magnetization for materials with spins deriving from organic species, i.e. with

Table 3. Compounds Exhibiting Photoinduced Change in Magnetic Properties

Nagai et al.[145]
MnTPP-TCNE

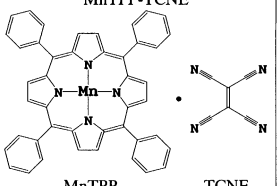

MnTPP TCNE
Photo-induced spin-flopping transition.

Pejakovic et al.[146]

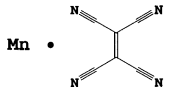

$Mn \cdot (TCNE)_x \cdot y(CH_2Cl_2)$

Sastry et al.[161]
$(NBu_4)_2Mn_2[Cu(opba)]_3 \cdot 6DMSO \cdot 1H_2O$

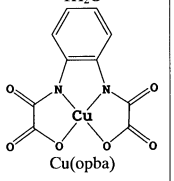

Cu(opba)

Ohkoshi et al.[152,153]

Schematic diagram of mixed ferro-ferrimagnet exhibiting photinduced magnetic pole inversion.

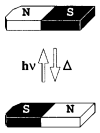

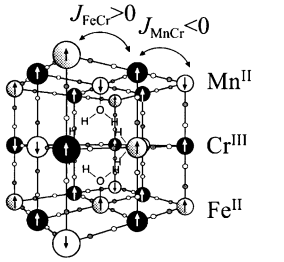

$J_{FeCr}>0$ $J_{MnCr}<0$
Mn^{II}
Cr^{III}
Fe^{II}

Rombaut et al.[155,156], Ohkoshi et al.[158]

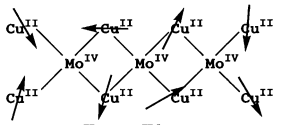

$Cu^{II}_2[Mo^{IV}(CN)_8]$
Paramagnet

hυ IVCT ⊿

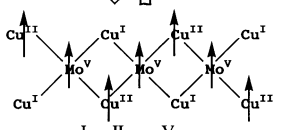

$Cu^{I}Cu^{II}[Mo^{V}(CN)_8]$
Ferromagnet

Schematic view of magnetic coupling in $Cu^{II}_2[Mo^{IV}(CN)_8] \cdot zH_2O$.

Sano et al.[147]

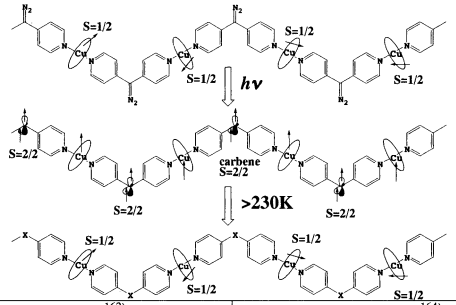

Berard et al.[162]

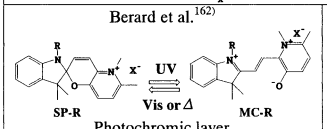

Photochromic layer.

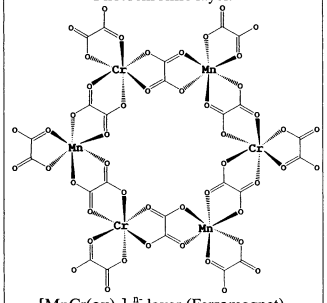

$[MnCr(ox)_3]_n^{n-}$ layer (Ferromagnet).

Einaga et al.[164]

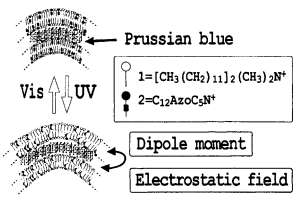

Schematic illustration of the molecule-based magnet.

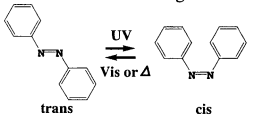

Gu et al.[165,166]

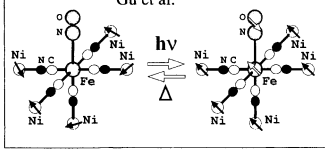

Spins on Ni are randomly oriented around an iron without net spin, while after illumination, they are ordered around an iron with spin and form a magnetic cluster.

Zhang et al.[167]

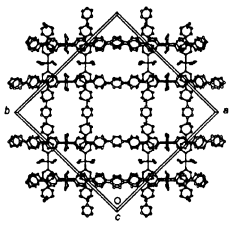

$CuCl_4$-BPyP has a logs–stacking structure with multichannels along c-axis.

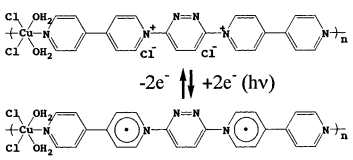

Photoreduction of $CuCl_4$-BPyP.

Hayami et al.[29]
LIESST : Highest relaxation temperature T=130K.

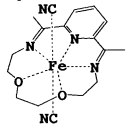

$Fe(L)(CN)_2 \cdot H_2O$
L=macrocyclic schiff-base ligand

Renz et al.[170]
Strong field LIESST.

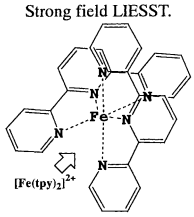

$[Fe_{0.02}Mn_{0.98}(tpy)_2](ClO_4)_2$

Létard et al.[168]

Light induced pair spin state.

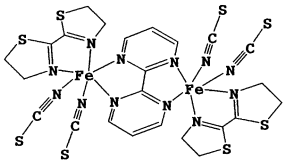

$[Fe(bt)(NCS)_2]_2 \cdot bpym$

Breuning et al.[171]
LIESST in a supramolecular $Fe^{II}_4[2 \times 2]$ grid.

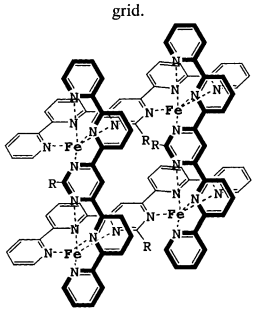

$[Fe_4L_4](ClO_4)_8$
L=4,6-bis(2,2"-bipyrid-6'-yl)-2-phenyl -pyrimidine

Corvaja et al.[172]
Excited quartet state of radical-excited triplet pair.

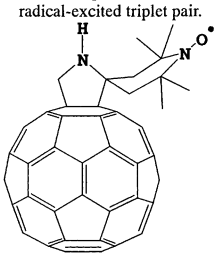

3,4-fulleropyrrolidine-2-spiro-4' -[2',2',6',6'-tetramethyl] piperidine-1'-oxyl

Teki et al.[176,177]
Excited quartet (s=3/2) state.

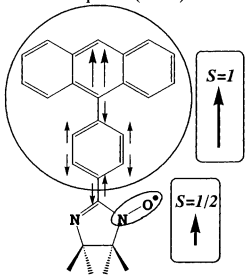

9-[4-(4,4,5,5-tetramethyl-1-yloxyimidazolin-2-yl)-phenyl]anthracene

Ishii et al.[173-175]
Excited quartet state.

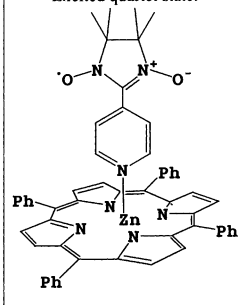

ZnTPP

Matsuda et al.[179-182]

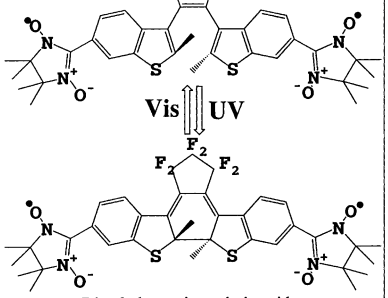

Diarylethene nitronyl nitroxide

Table 3. (Continued)

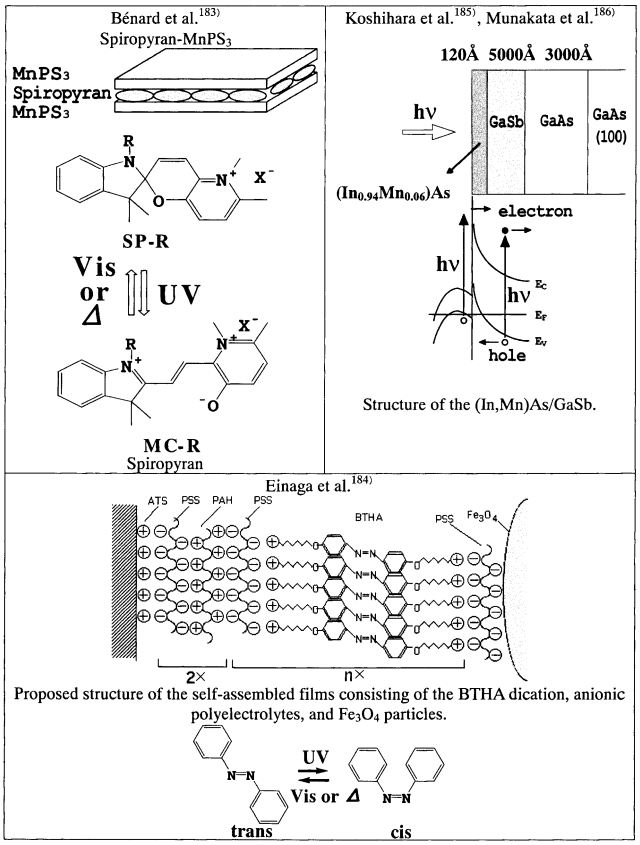

spins supplied by electrons in π orbitals. Furthermore, a persistent photoinduced change in magnetization has been reported by Sano et al. They showed the formation of ferromagnetic chains via the photochemical generation of a triplet carbene at low temperature.[147] Recently, Karasawa et al. showed that the photoinduced state in the related compound has spin-glass-like magnetic properties.[151]

Another interesting phenomenon is a photo-induced magnetic pole inversion in a ferro-ferrimagnet, $(Fe_x^{II}Mn_{1-x}^{II})[Cr^{III}(CN)_6]\cdot 7.5H_2O$, through a combination of mixed ferro-ferrimagnetism and photomagnetism.[152,153] This effect, reported by Ohkoshi et al., is important from the viewpoint of its applications as well as its more fundamental aspects. Furthermore, it has been reported that CuMo octa-cyanides, CoW octa-cyanides and MnCu bimetallic compounds also exhibit a photoinduced magnetization effect.[154–161] These photomagnetic effects in the octa-cyanides are thought to be caused by a photoinduced electron transfer between Cu and Mo and between Co and W, respectively.

Bénard et al. have synthesized a photochromic molecule-based magnet with alternating ferromagnetic and photochromic layers.[162] UV irradiation transforms the initially very soft magnet to a much harder one by considerably increasing its coercive field as well as the remnant magnetization, although the change is irreversible. A spectacular change in the hysteresis loop was ascribed to photoinduced defects in the crystal structure through the photoreaction of a spiropyran derivative. Einaga et al. also reported a composite of molecule-based magnets and photochromic dyes.[164] They inserted Prussian blue into azobenzene containing multiple layer vesicles. When the composite is illuminated by UV and visible light at low temperature, trans-cis photoisomerization of azobenzene is induced in the vesicle. The structural changes in the vesicle affect the electronic structure of the Prussian blue to some extent, which results in a reversible change in the magnetization value. Gu et al. constructed a photo-switchable spin device, $Ni^{II}[Fe^{II}(CN)_5NO]$, by taking advantage of the photochromic property of $[Fe(CN)_5NO]^{2-}$.[165,166] They showed that the excitation of the MLCT band results in the formation of magnetic clusters with $S = 5$. Furthermore, Zhang et al. synthesized a photo-responsive Cu complex with a redox-active ligand.[167] When the coordination polymer was illuminated, the magnetization value was changed because of a photoinduced electron transfer from the chloride ion to the redox active ligand.

In the field of photoinduced spin transition, several interesting phenomena have recently been discovered. It has been believed that the photoinduced high-spin state relaxes back to the original low-spin state below 80 K. On the other hand, Hayami et al. have achieved a higher relaxation temperature, 130 K, in an Fe^{II} complex.[29] To the best of our knowledge, 130 K is the highest relaxation temperature reported so far. Létard et al reported an unusual example of photomagnetic behaviour stemming from the interplay between the spin-crossover and magnetic coupling phenomena.[168] They showed that the magnetic properties of their binuclear Fe^{II} complex changed from the $S = 0$ spin state of the LS–LS pair to the $S = 0$ spin state of the HS–HS pair by illumination. Renz et al. reported the observation of LIESST effects for a strong ligand-field complex of Fe^{II}.[170] Based on the LIESST state relaxation model, it has been believed that LIESST effects could not be observed for such a strong-field Fe^{II} complex. Hence, their result is an astonishing one. Furthermore, the observation of the LIESST effect in a supramolecular system with an $Fe_4^{II}[2\times 2]$ grid structure was recently reported by Breuning et al.[171]

An excited high-spin state induced by illumination has been recently investigated using time-resolved electron spin resonance. Corvaja et al. have reported an excited quartet state for a radical-excited triplet pair in a fullerene-mononitroxide radical system in solution.[172] Ishii et al. reported the observation of a quartet state in a sample of tetraphenylporphinatozinc(II) coordinated by *p*-pyridyl nitronyl-nitroxide in the solid phase.[173] They also reported novel photo-magnetic properties, i.e. photoinduced population transfer between the singlet ground state and triplet ground state.[174] Teki et al. reported quartet excited spin states in purely organic π-conjugated spin systems.[176] Furthermore, the first excited quintet state was reported for a bis-adduct of fullerene with two nitroxide radicals at the *trans*-3 position by Mizouchi et al.[178] These studies provide important information on novel spin alignment, and they lead to a new strategy for photoinduced magnetic spin systems.

Matsuda et al. showed reversible photoswitching in an intramolecular magnetic interaction.[179–182] They constructed a bis(nitronyl nitroxide) with diarylethene as a photoswitching core. When this is illuminated by UV and visible light, the magnetic exchange interaction between the two nitronyl nitroxide radicals is modified because of the photo-isomerization of the photochromic spin coupler. Their approach may lead to

the development of photo-switchable molecular logic circuits.

Photoinduced changes in the magnetic properties were also observed for spiropyran-$MnPS_3$ intercalation compounds,[183] iron oxide particles in self-assembled films containing azobenzene,[184] diluted magnetic semiconductor heterostructures of (In, Mn)As/GaSb,[185,186] spinel ferrite films with spin glass state,[187,188] EuO nanocrystals,[189] and doped manganites, i.e. $(Nd_{0.5}Sm_{0.5})_{0.6}Sr_{0.4}MnO_3$[190] although these are not molecule-based magnets. It is important to note that the magnetic properties in the composite of the iron oxide and azobenzene could be modified even at room temperature.[184]

6. Conclusion

We have described molecule-based magnets, i.e. Prussian blue analogues, whose magnetic properties can be controlled between the ferro- or ferri-magnetic and the para- or dia-magnetic by electrochemical treatment and by illumination. Furthermore, we have shown that Co valence tautomeric compounds, $[Co^{III\text{-}LS}(dbsq)(dbcat)(NN)]$, an Fe^{III} complex, $[Fe^{III\text{-}LS}(pap)_2]ClO_4 \cdot H_2O$, and a Cu^{II} complex, $[Cu^{II}(dieten)_2](BF_4)_2$, exhibit a long-lived metastable state. The development of such tunable molecular compounds is important because of their fundamental aspects as well as their potential applications such as optical memory.

It is important to emphasize again that our strategy for achieving a long-lived photoinduced metastable state after illumination is the introduction of an inter-molecular interaction using coordinate bonding (FeCo Prussian blue), ligand-to-ligand interlocking (Co valence tautomeric compounds), π–π interaction (an Fe^{III} spin-crossover complex) and hydrogen bonding (a Cu^{II} thermochromic complex). This is because the cooperativity resulting from the molecular interaction operates to increase the activation energy for the relaxation processes, potentially enabling the observation of a long-lived metastable state. This means that optically-switchable molecular solids could be developed by mixing our knowledge of photochemistry and supramolecular chemistry. We believe that our approach can be widely applied in the design of a variety of optically switchable molecular compounds.

The authors thank all of our co-workers and we acknowledge financial support in part by the Collaboration of Regional Entities for the Advancement of Technological Excellence.

References

1 D. R. Bloomquist and R. D. Willett, *Coord. Chem. Rev.*, **47**, 125 (1982).

2 K. Itaya, I. Uchida, and V. D. Neff, *Acc. Chem. Res.*, **19**, 162 (1986).

3 P. Gütlich, A. Hauser, and H. Spiering, *Angew. Chem., Int. Ed. Engl.*, **33**, 2024 (1994).

4 O. Sato, T. Iyoda, A. Fujishima, and K. Hashimoto, *Science*, **271**, 49 (1996).

5 O. Sato, Z.-Z. Gu, H. Etoh, J. Ichiyanagi, T. Iyoda, A. Fujishima, and K. Hashimoto, *Chem. Lett.*, **1997**, 37.

6 O. Sato, T. Iyoda, A. Fujishima, and K. Hashimoto, *Science*, **272**, 704 (1996).

7 O. Sato, Y. Einaga, T. Iyoda, A. Fujishima, and K. Hashimoto, *J. Electrochem. Soc.*, **144**, L11 (1997).

8 O. Sato, Y. Einaga, T. Iyoda, A. Fujishima, and K. Hashimoto, *J. Phys. Chem. B*, **101**, 3903 (1997).

9 O. Sato, Y. Einaga, T. Iyoda, A. Fujishima, and K. Hashimoto, *Inorg. Chem.*, **38**, 4405 (1999).

10 Y. Einaga, Z.-Z. Gu, Y. Kobayashi, O. Sato, T. Iyoda, F. Ambe, K. Hashimoto, and A. Fujishima, *Riken Review*, **16**, 43 (1997).

11 Y. Einaga, O. Sato, T. Iyoda, K. Kobayashi, F. Ambe, K. Hashimoto, and A. Fujishima, *Riken Review*, **16**, 41 (1997).

12 Y. Einaga, S. Ohkoshi, O. Sato, A. Fujishima, and K. Hashimoto, *Chem. Lett.*, **1998**, 585.

13 Y. Einaga, Z.-Z. Gu, Y. Kobayashi, O. Sato, T. Iyoda, F. Ambe, K. Hashimoto, and A. Fujishima, *Hyperfine Interact.*, **116**, 159 (1998).

14 Y. Einaga, O. Sato, T. Iyoda, K. Kobayashi, F. Ambe, K. Hashimoto, and A. Fujishima, *Hyperfine Interact., C*, **3**, 236 (1998).

15 N. Shimamoto, S. Ohkoshi, O. Sato, and K. Hashimoto, *Mol. Cryst. Liq. Cryst.*, **344**, 95 (2000).

16 N. Shimamoto, S. Ohkoshi, O. Sato, and K. Hashimoto, *Inorg. Chem.*, **41**, 678 (2002).

17 T. Yokoyama, T. Ohta, O. Sato, and K. Hashimoto, *Phys. Rev. B*, **58**, 8257 (1998).

18 T. Yokoyama, M. Kiguchi, T. Ohta, O. Sato, Y. Einaga, and K. Hashimoto, *Phys. Rev. B*, **60**, 9340 (1999).

19 K. Seki, S. Hayami, A. Fujishima, and O. Sato, The 79th Annual Meeting of the Chemical Society of Japan, Vol. 1, p. 57, Kobe, 2001.

20 O. Sato, S. Hayami, Z.-Z. Gu, K. Seki, R. Nakajima, and A. Fujishima, *Chem. Lett.*, **2001**, 874.

21 T. Yokoyama, K. Okamoto, K. Nagai, T. Ohta, S. Hayami, Z.-Z. Gu, R. Nakajima, and O. Sato, *Chem. Phys. Lett.*, **345**, 272 (2001).

22 O. Sato, S. Hayami, Z.-Z. Gu, K. Takahashi, R. Nakajima, K. Seki, and A. Fujishima, *J. Photochem. Photobiol. A., Chem.*, **149**, 111 (2002).

23 O. Sato, S. Hayami, Z.-Z. Gu, K. Takahashi, R. Nakajima, and A. Fujishima, *Chem. Phys. Lett.*, **355**, 169 (2002).

24 O. Sato, S. Hayami, Z.-Z. Gu, K. Takahashi, R. Nakajima, K. Seki, and A. Fujishima, *Phase Transitions*, in press.

25 S. Hayami, Z.-Z. Gu, M. Shiro, Y. Einaga, A. Fujishima, and O. Sato, *J. Am. Chem. Soc.*, **122**, 7126 (2000).

26 K. Takahashi, R. Nakajima, Z.-Z. Gu, H. Yoshiki, A. Fujishima, and O. Sato, *Chem. Commun.*, **2002**, 1578.

27 S. Hayami, Z.-Z. Gu, Y. Einaga, A. Fujishima, and O. Sato, *J. Am. Chem. Soc.*, **123**, 11644 (2001).

28 S. Hayami, Z.-Z. Gu, Y. Einaga, A. Fujishima, and O. Sato, *Mol. Cryst. Liq. Cryst.*, **343**, 65 (2000).

29 S. Hayami, Z.-Z. Gu, Y. Einaga, Y. Kobayashi, Y. Ishikawa, Y. Yamada, A. Fujishima, and O. Sato, *Inorg. Chem.*, **40**, 3240 (2001).

30 S. Schenker and A. Hauser, *J. Am. Chem. Soc.*, **116**, 5497 (1994).

31 O. Kahn, "Molecular Magnetism," VCH, New York (1993).

32 J. S. Miller and A. J. Epstein, *Angew. Chem., Int. Ed. Engl.*, **33**, 385 (1994).

33 M. Ohba and H. Okawa, *Coord. Chem. Rev.*, **198**, 313 (2000).

34 A. N. Holden, B. T. Matthias, P. W. Anderson, and H. W.

Lewis, *Phys. Rev.*, **102**, 1463 (1956).
35 R. M. Bozorth, H. J. Williams, and D. E. Walsh, *Phys. Rev.*, **103**, 572 (1956).
36 A. Ito, M. Suenaga, and K. Ono, *J. Chem. Phys.*, **48**, 3597 (1968).
37 F. Herren, P. Fischer, A. Ludi, and W. Halg, *Inorg. Chem.*, **19**, 956 (1980).
38 V. Gadet, T. Mallah, I. Castro, M. Verdaguer, and P. Veillet, *J. Am. Chem. Soc.*, **114**, 9213 (1992).
39 T. Mallah, S. Thiebaut, M. Verdaguer, and P. Veillet, *Science*, **262**, 1554 (1993).
40 S. Ferlay, T. Mallah, R. Ouahes, P. Veillet, and M. Verdaguer, *Nature*, **378**, 701 (1995).
41 W. R. Entley and G. S. Girolami, *Science*, **268**, 397 (1995).
42 S. H. Holmes and G. S. Girolami, *J. Am. Chem. Soc.*, **121**, 5593 (1999).
43 Φ. Hatlevik, W. E. Buschmann, J. Zhang, J. L. Manson, and J. S. Miller, *Adv. Mater.*, **11**, 914 (1999).
44 K. Itaya, K. Shibayama, H. Akahoshi, and S. Toshima, *J. Apply. Phys.*, **53**, 804 (1982).
45 W. E. Buschmann, S. C. Paulson, C. M. Wynn, M. A. Girtu, A. J. Epstein, H. S. White, and J. S. Miller, *Adv. Mater.*, **9**, 645 (1997).
46 W. E. Buschmann, S. C. Paulson, C. M. Wynn, M. A. Girtu, A. J. Epstein, H. S. White, and J. S. Miller, *Chem. Mater.*, **10**, 1386 (1998).
47 D. N. Hume and I. M. Kolthoff, *J. Am. Chem. Soc.*, **65**, 1897 (1943).
48 S. Ohkoshi, M. Mizuno, G. J. Hung, and K. Hashimoto, *J. Phys. Chem. B*, **104**, 9365 (2000).
49 K. Ikeda, S. Ohkoshi, and K. Hashimoto, *Chem. Phys. Lett.*, **349**, 371 (2001).
50 H. J. Buser, D. Schwarzenbach, W. Petter, and A. Ludi, *Inorg. Chem.*, **16**, 2704 (1977).
51 M. Nishino, S. Kubo, Y. Yoshioka, A. Nakamura, and K. Yamaguchi, *Mol. Cryst. Liq. Cryst.*, **305**, 109 (1997).
52 S. Ohkoshi and K. Hashimoto, *J. Photochem. Photobiol. C., Photochem. Rev.*, **2**, 71 (2001).
53 J. B. Goodenough, *J. Phys. Chem. Solids*, **6**, 287 (1958).
54 J. B. Goodenough, *Phys. Rev.*, **100**, 564 (1959).
55 J. Kanamori, *J. Phys. Chem. Solids*, **10**, 87 (1959).
56 A. P. Ginsberg, *Inorg. Chim. Acta. Rev.*, **5**, 45 (1971).
57 S. Ohkoshi, A. Fujishima, and K. Hashimoto, *J. Am. Chem. Soc.*, **120**, 5349 (1998).
58 S. Ohkoshi, Y. Einaga, A. Fujishima, and K. Hashimoto, *J. Electroanal. Chem.*, **473**, 245 (1999).
59 M. Mizuno, S. Ohkoshi, and K. Hashimoto, *Adv. Mater.*, **12**, 1955 (2000).
60 B. Mayoh and P. Day, *J. Chem. Soc., Dalton Trans.*, **1976**, 1483.
61 D. H. Huchital and R. J. Hodges, *Inorg. Chem.*, **12**, 998 (1973).
62 S. Bagger and K. Gibson, *Acta Chem. Scand.*, **27**, 3227 (1973).
63 A. Vogler, A. H. Osman, and H. Kunkely, *Coord. Chem. Rev.*, **64**, 159 (1985).
64 A. Vogler and H. Kunkely, *Ber. Bunsen-Ges. Phys. Chem.*, **79**, 301 (1975).
65 R. E. Hester and E. M. Nour, *J. Chem. Soc., Dalton Trans.*, **1981**, 939.
66 G. Visalakshi and K. S. Venkathswarlu, *Proc. Indian. Acad. Sci.*, **91**, 213 (1982).
67 S. Bagger and P. Stoltze, *Acta Chem. Scand. A*, **37**, 247 (1983).
68 P. V. Bernhardt and M. Martinez, *Inorg. Chem.*, **38**, 424 (1999).
69 P. V. Bernhardt, B. P. Macpherson, and M. Martinez, *Inorg. Chem.*, **39**, 5203 (2000).
70 Z. Gao, X. Zhou, G. Wang, P. Li, and Z. Zhao, *Anal. Chim. Acta*, **244**, 39 (1991).
71 Z. Gao, G. Wang, P. Li, and Z. Zhao, *Electrochim. Acta*, **36**, 147 (1991).
72 J. Joseph, H. Gomathi, and G. P. Rao., *J. Electroanal. Chem.*, **304**, 263 (1991).
73 Z. Gao, J. Bobacka, and A. Ivaska, *Electrochim. Acta*, **38**, 379 (1993).
74 P. J. Kulesza, M. A. Malik, S. Zamponi, M. Berrettoni, and R. Marassi, *J. Electroanal. Chem.*, **397**, 287 (1995).
75 P. J. Kulesza, M. A. Malik, K. Miecznikowski, A. Wolkiewicz, S. Zamponi, M. Berrettoni, and R. Marassi, *J. Electrochem. Soc.*, **143**, L10 (1996).
76 P. J. Kulesza, M. A. Malik, M. Berrettoni, M. Giorgetti, S. Zamponi, R. Schmidt, and R. Marassi, *J. Phys. Chem. B*, **102**, 1870 (1998).
77 P. J. Kulesza, S. Zamponi, M. A. Maki, M. Berrettoni, A. Wolkiewicz, and R. Marassi, *Electrochim. Acta*, **43**, 919 (1998).
78 R. O. Lezna, R. Romagnoli, N. R. d. Tacconi, and K. Rajeshwar, *J. Phys. Chem. B*, **106**, 3612 (2002).
79 In our previous paper, we tried to fit the Mössbauer spectra of cobalt-iron cyanides, which have the $Fe^{II}(t_{2g}{}^6e_g{}^0)$-CN-$Co^{III\text{-}LS}$-$(t_{2g}{}^6e_g{}^0)$ structure, with one line, and by assuming a zero quadrupole interaction. However, it was found that the spectra could not be fitted properly. Therefore, we achieved a fit for the Mössbauer spectra by using a symmetric quadrupole doublet.
80 D. M. Adams, A. Dei, A. L. Rheingold, and D. N. Hendrickson, *J. Am. Chem. Soc.*, **115**, 8221 (1993).
81 T. Kawamoto, Y. Asai, and S. Abe, *Phys. Rev. B*, **60**, 12990 (1999).
82 D. A. Pejakovic, J. L. Manson, J. S. Miller, and A. J. Epstein, *J. Apply. Phys.*, **87**, 6028 (2000).
83 D. A. Pejakovic, J. L. Manson, J. S. Miller, and A. J. Epstein, *J. Apply. Phys.*, **88**, 4457 (2000).
84 D. A. Pejakovic, J. L. Manson, J. S. Miller, and A. J. Epstein, *Phys. Rev. Lett.*, **85**, 1994 (2000).
85 D. A. Pejakovic, J. L. Manson, J. S. Miller, and A. J. Epstein, *Synth. Met.*, **122**, 529 (2001).
86 D. A. Pejakovic, J. L. Manson, C. Kitamura, J. S. Miller, and A. J. Epstein, *Polyhedron*, **20**, 1435 (2001).
87 F. Varret, H. Constant-Machado, J. L. Dormann, A. Goujon, J. Jeftic, M. Nogues, A. Bousseksou, S. Klokishner, A. Dorbecq, and M. Verdaguer, *Hyperfine Interact.*, **113**, 37 (1998).
88 E. Codjovi, W. Morscheidt, J. Jeftic, J. Linares, M. Nogues, A. Goujon, O. Roubeau, H. Constant-Machado, A. Desaix, A. Bousseksou, M. Verdaguer, and F. Varret, *Mol. Cryst. Liq. Cryst.*, **334**, 1295 (1999).
89 A. Bleuzen, C. Lomenech, A. Dolbecq, F. Villain, A. Goujon, O. Roubeau, M. Nogues, F. Varret, F. Baudelet, E. Dartyge, C. Giorgetti, J. J. Gallet, C. C. Moulin, and M. Verdaguer, *Mol. Cryst. Liq. Cryst.*, **335**, 253 (1999).
90 A. Bleuzen, C. Lomenech, V. Escax, F. Villain, F. Varret, M. C. C. Moulin, and M. Verdaguer, *J. Am. Chem. Soc.*, **122**, 6648 (2000).

91 A. Goujon, O. Roubeau, F. Varret, A. Dolbecq, A. Bleuzen, and M. Verdaguer, *Eur. Phys. J. B*, **14**, 115 (2000).
92 A. Goujon, F. Varret, V. Escax, A. Bleuzen, and M. Verdaguer, *Polyhedron*, **20**, 1347 (2001).
93 F. Varret, A. Goujon, and A. Bleuzen, *Hyperfine Interact.*, **134**, 69 (2001).
94 G. Champion, V. Escax, C. C. Moulin, A. Bleuzen, F. Villain, F. Baudelet, E. Dartyge, and M. Verdaguer, *J. Am. Chem. Soc.*, **123**, 12544 (2001).
95 C. C. Moulin, F. Villain, A. Bleuzen, M.-A. Arrio, P. Sainctavit, C. Lomenech, V. Escax, F. Baudelet, E. Dartyge, J.-J. Gallet, and M. Verdaguer, *J. Am. Chem. Soc.*, **122**, 6653 (2000).
96 G. L. Gutesev, B. V. Reddy, S. N. Khanna, B. K. Rao, and P. Jena, *Phys. Rev. B*, **58**, 14131 (1998).
97 K. Yoshizawa, F. Mohri, G. Nuspl, and T. Yamabe, *J. Phys. Chem. B*, **102**, 5432 (1998).
98 M. Nishino, K. Yamaguchi, and S. Miyashita, *Phys. Rev. B*, **58**, 9303 (1998).
99 M. Nishino, Y. Kitagawa, T. Onishi, T. Soda, Y. Takano, H. Nagao, Y. Yoshioka, and K. Yamaguchi, *Mol. Cryst. Liq. Cryst.*, **343**, 469 (2000).
100 T. Kawamoto, Y. Asai, and S. Abe, *J. Lumin.*, **87–89**, 658 (2000).
101 T. Kawamoto, Y. Asai, and S. Abe, *Phys. Rev. Lett.*, **86**, 348 (2001).
102 T. Kawamoto and S. Abe, *Phase Transitions*, **74**, 209 (2001).
103 V. Escax, A. Bleuzen, C. C. Moulin, F. Villain, A. Goujon, F. Varret, and M. Verdaguer, *J. Am. Chem. Soc.*, **123**, 12536 (2001).
104 A. Goujon, F. Varret, V. Escax, A. Bleuzen, and M. Verdaguer, *Polyhedron*, **20**, 1339 (2001).
105 R. A. Marcus, *J. Chem. Phys.*, **24**, 966 (1956).
106 R. M. Buchanan and C. G. Pierpont, *J. Am. Chem. Soc.*, **102**, 4951 (1980).
107 C. G. Pierpont and R. M. Buchanan, *Coord. Chem. Rev.*, **38**, 45 (1981).
108 C. G. Pierpont and C. W. Lange, *Prog. Inorg. Chem.*, **41**, 331 (1994).
109 C. G. Pierpont and A. S. Attia, *Collect. Czech. Chem. Commun.*, **66**, 33 (2001).
110 C. G. Pierpont, *Coord. Chem. Rev.*, **216–217**, 99 (2001).
111 C. G. Pierpont, *Coord. Chem. Rev.*, **219–221**, 415 (2001).
112 D. M. Adams, A. Dei, A. L. Rheingold, and D. N. Hendrickson, *Angew. Chem., Int. Ed. Engl.*, **32**, 880 (1993).
113 D. M. Adams, B. Li, J. D. Simon, and D. N. Hendrickson, *Angew. Chem., Int. Ed. Engl.*, **34**, 1481 (1995).
114 D. M. Adams and D. N. Hendrickson, *J. Am. Chem. Soc.*, **118**, 11515 (1996).
115 D. M. Adams, L. Noodleman, and D. N. Hendrickson, *Inorg. Chem.*, **36**, 3966 (1997).
116 O.-S. Jung, D. H. Jo, Y. S. Sohn, and C. G. Pierpont, *Angew. Chem., Int. Ed. Engl.*, **35**, 1694 (1996).
117 O.-S. Jung, D. H. Jo, Y.-A. Lee, Y. S. Sohn, and C. G. Pierpont, *Inorg. Chem.*, **37**, 5875 (1998).
118 P. J. Crowley and H. M. Haendler, *Inorg. Chem.*, **1**, 904 (1962).
119 D. H. Jo, J. H. Jeong, H. J. Yeo, Y. S. Sohn, and O.-S. Jung, *Bull. Korean Chem. Soc.*, **16**, 504 (1995).
120 C. Roux, D. M. Adams, J. P. Itie, A. Polian, D. N. Hendrickson, and M. Verdaguer, *Inorg. Chem.*, **35**, 2846 (1996).
121 C. Roux, J. Zarembowitch, J. P. Itie, M. Verdaguer, E. Dartyge, A. Fontaine, and H. Tolentino, *Inorg. Chem.*, **30**, 3174 (1991).
122 M. W. Lynch, R. M. Buchanan, C. G. Pierpont, and D. N. Hendrickson, *Inorg. Chem.*, **20**, 1038 (1981).
123 G. A. Abakumov and V. I. Nevodchikov, *Dokl. Akad. Nauk, SSSR*, **266**, 1407 (1982).
124 C. W. Lange, M. Földeàki, V. I. Nevodchikov, V. K. Cherkasov, G. A. Abakumov, and C. G. Pierpont, *J. Am. Chem. Soc.*, **114**, 4220 (1992).
125 G. A. Abakumov, V. K. Cherkasov, M. P. Bubnov, O. G. Ellert, G. V. Dobrohotova, L. N. Zahalov, and Y. T. Struchkov, *Dokl. Akad. Nauk, SSSR*, **328**, 332 (1993).
126 O.-S. Jung and C. G. Pierpont, *J. Am. Chem. Soc.*, **116**, 2229 (1994).
127 L. A. Vermeulen and M. E. Thompson, *Nature*, **358**, 656 (1992).
128 P. Dutta, *Nature*, **358**, 621 (1992).
129 S. Decurtins, P. Gütlich, C. P. Kohler, H. Spiering, and A. Hauser, *Chem. Phys. Lett.*, **105**, 1 (1984).
130 H. Oshio, K. Kitazaki, J. Mishiro, N. Kato, Y. Maeda, and Y. Takashima, *J. Chem. Soc., Dalton Trans.*, **1987**, 1341.
131 S. Schenker, A. Hauser, and R. M. Dyson, *Inorg. Chem.*, **35**, 4676 (1996).
132 K. Sone and Y. Fukuda, "Inorganic Thermochromism," Springer (1987).
133 P. Pfeiffer and H. Glaser, *J. Prakt. Chem.*, **151**, 134 (1938).
134 B. Narayanan and M. M. Bhadbhade, *J. Coord. Chem.*, **46**, 115 (1998).
135 B. P. Kennedy and A. B. P. Lever, *J. Am. Chem. Soc.*, **95**, 6907 (1973).
136 A. Nishimori, E. A. Schmitt, D. N. Hendrickson, and M. Sorai, *J. Phys. Chem. Solids*, **55**, 99 (1994).
137 A. B. P. Lever, E. Mantovani, and J. C. Donini, *Inorg. Chem.*, **10**, 2424 (1971).
138 A. B. P. Lever and E. Mantovani, *Inorg. Chem.*, **10**, 817 (1971).
139 L. Fabbrizzi, M. Micheloni, and P. Paoletti, *Inorg. Chem.*, **13**, 3019 (1974).
140 J. R. Ferraro, L. J. Basile, L. R. Garcia-ineguez, P. Paoletti, and L. Fabbrizzi, *Inorg. Chem.*, **15**, 2342 (1976).
141 K. L. Bray, H. G. Drickamer, E. A. Schmitt, and D. N. Hendrickson, *J. Am. Chem. Soc.*, **111**, 2849 (1989).
142 I. Grenthe, P. Paoletti, M. Sandstrom, and S. Ginkberg, *Inorg. Chem.*, **18**, 2687 (1979).
143 M. M. Andino, J. D. Curet, M. M. Muir, and R. C. Ryan, *Acta. Crystallogr. Sect. B*, **32**, 3185 (1976).
144 P. Gütlich, Y. Garcia, and T. Woike, *Coord. Chem. Rev.*, **219–221**, 839 (2001).
145 K. Nagai, T. Iyoda, A. Fujishima, and K. Hashimoto, *Solid. State. Commun.*, **102**, 809 (1997).
146 D. A. Pejakovic, C. Kitamura, J. S. Miller, and A. J. Epstein, *Phys. Rev. Lett.*, **88**, 7202 (2002).
147 Y. Sano, M. Tanaka, N. Koga, K. Matsuda, H. Iwamura, P. Rabu, and M. Drillon, *J. Am. Chem. Soc.*, **119**, 8246 (1997).
148 N. Koga and H. Iwamura, *Mol. Cryst. Liq. Cryst.*, **305**, 415 (1997).
149 S. Karasawa, M. Tanaka, N. Koga, and H. Iwamura, *Chem. Commun.*, **1997**, 1359.
150 S. Karasawa, Y. Sano, T. Akita, N. Koga, T. Itoh, H. Iwamura, P. Rabu, and M. Drillon, *J. Am. Chem. Soc.*, **120**, 10080

(1998).
151 S. Karasawa, H. Kumada, N. Koga, and H. Iwamura, *J. Am. Chem. Soc.*, **123**, 9685 (2001).
152 S. Ohkoshi, S. Yorozu, O. Sato, T. Iyoda, A. Fujishima, and K. Hashimoto, *Appl. Phys. Lett.*, **70**, 1040 (1997).
153 S. Ohkoshi and K. Hashimoto, *J. Am. Chem. Soc.*, **121**, 10591 (1999).
154 G. Rombaut, S. Golhen, L. Ouahab, C. Mathoniere, and O. Kahn, *J. Chem. Soc., Dalton Trans.*, **2000**, 3609.
155 G. Rombaut, C. Mathoniere, P. Guionneau, S. Golhen, L. Ouahab, M. Verelst, and P. Lecante, *Inorg. Chim. Acta*, **326**, 27 (2001).
156 G. Rombaut, M. Verelst, S. Golhen, L. Ouahab, C. Mathoniere, and O. Kahn, *Inorg. Chem.*, **40**, 1151 (2001).
157 S. Ohkoshi, N. Machida, Y. Abe, Z. J. Zhong, and K. Hashimoto, *Chem. Lett.*, **2001**, 312.
158 S. Ohkoshi, N. Machida, Z. J. Zhong, and K. Hashimoto, *Synth. Met.*, **122**, 523 (2001).
159 T. Yokoyama, K. Okamoto, D. Matsumura, T. Ohta, S. Ohkoshi, and K. Hashimoto, *J. Synchrotron Rad.*, **8**, 913 (2001).
160 T. Yokoyama, K. Okamoto, T. Ohta, S. Ohkoshi, and K. Hashimoto, *Phys. Rev. B*, **65**, 064438 (2002).
161 M. D. Sastry, M. K. Bhide, R. M. Kadam, S. A. Chavan, J. V. Yakhmi, and O. Kahn, *Chem. Phys. Lett.*, **301**, 385 (1999).
162 S. Bénard, E. Rivière, P. Yu, K. Nakatani, and F. Delouis, *Chem. Mater.*, **13**, 159 (2001).
163 K. Nakatani and P. Yu, *Adv. Mater.*, **13**, 1411 (2001).
164 Y. Einaga, O. Sato, T. Iyoda, A. Fujishima, and K. Hashimoto, *J. Am. Chem. Soc.*, **121**, 3745 (1999).
165 Z.-Z. Gu, O. Sato, T. Iyoda, K. Hashimoto, and A. Fujishima, *J. Phys. Chem.*, **100**, 18289 (1996).
166 Z.-Z. Gu, O. Sato, T. Iyoda, K. Hashimoto, and A. Fujishima, *Chem. Mater.*, **9**, 1092 (1997).
167 J. Zhang, M. M. Matsushita, X. X. Kong, J. Abe, and T. Iyoda, *J. Am. Chem. Soc.*, **123**, 12105 (2001).
168 J. F. Létard, J. A. Real, N. Moliner, A. B. Gaspar, L. Capes, O. Cador, and O. Kahn, *J. Am. Chem. Soc.*, **121**, 10630 (1999).
169 G. Chastanet, A. B. Gaspar, J. A. Real, and J. F. Létard, *Chem. Commun.*, **2001**, 819.
170 F. Rentz, H. Oshio, V. Ksenofontov, M. Waldeck, H. Spiering, and P. Gütlich, *Angew. Chem., Int. Ed.*, **39**, 3699 (2000).
171 E. Breuning, M. Ruben, J. M. Lehn, F. Renz, Y. Garcia, V. Ksenofontov, P. Gütlich, E. Wegelius, and K. Rissanen, *Angew. Chem., Int. Ed.*, **39**, 2504 (2000).
172 C. Corvaja, M. Maggini, M. Prato, G. Scorrano, and M. Venzin, *J. Am. Chem. Soc.*, **117**, 8857 (1995).
173 K. Ishii, J. Fujisawa, Y. Ohba, and S. Yamauchi, *J. Am. Chem. Soc.*, **118**, 13079 (1996).
174 K. Ishi, Y. Hirose, and N. Kobayashi, *J. Am. Chem. Soc.*, **120**, 10551 (1998).
175 K. Ishii, J. Fujisawa, A. Adachi, S. Yamauchi, and N. Kobayashi, *J. Am. Chem. Soc.*, **120**, 3152 (1998).
176 Y. Teki, S. Miyamoto, K. Iimura, M. Nakatsuji, and Y. Miura, *J. Am. Chem. Soc.*, **122**, 984 (2000).
177 Y. Teki, S. Miyamoto, M. Nakatsuji, and Y. Miura, *J. Am. Chem. Soc.*, **123**, 294 (2001).
178 N. Mizouchi, Y. Ohba, and S. Yamauchi, *J. Phys. Chem. A*, **103**, 7749 (1999).
179 K. Matsuda and M. Irie, *J. Am. Chem. Soc.*, **122**, 7195 (2000).
180 K. Matsuda and M. Irie, *J. Am. Chem. Soc.*, **122**, 8309 (2000).
181 K. Matsuda and M. Irie, *Chem. Eur. J.*, **7**, 3466 (2001).
182 K. Matsuda and M. Irie, *J. Am. Chem. Soc.*, **123**, 9896 (2001).
183 S. Bénard, A. Léaustic, E. Rivière, P. Yu, and R. Clément, *Chem. Mater.*, **13**, 3709 (2001).
184 Y. Einaga, Z.-Z. Gu, S. Hayami, A. Fujishima, and O. Sato, *Thin Solid Films*, **374**, 109 (2000).
185 S. Koshihara, A. Oiwa, M. Hirasawa, S. Katsumoto, Y. Iye, C. Urano, H. Takagi, and M. Munekata, *Phys. Rev. Lett.*, **78**, 4617 (1997).
186 H. Munekata, T. Abe, S. Koshihara, A. Oiwa, M. Hirasawa, S. Katsumoto, Y. Iye, C. Urano, and H. Takagi, *J. Apply. Phys.*, **81**, 4862 (1997).
187 Y. Muraoka, H. Tabata, and T. Kawai, *Appl. Phys. Lett.*, **76**, 1179 (2000).
188 Y. Muraoka, H. Tabata, and T. Kawai, *Appl. Phys. Lett.*, **77**, 4016 (2000).
189 Y. Hasegawa, S. Thongchant, Y. Wada, H. Tanaka, T. Kawai, T. Sakata, H. Mori, and S. Yanagida, *Angew. Chem., Int. Ed.*, **41**, 2073 (2002).
190 K. Matsuda, A. Machida, Y. Moritomo, and A. Nakamura, *Phys. Rev. B*, **58**, R4203 (1998).
191 T. Kawamoto, Y. Asai, and S. Abe, *Mol. Cryst. Liq. Cryst.*, **376**, 423 (2002).

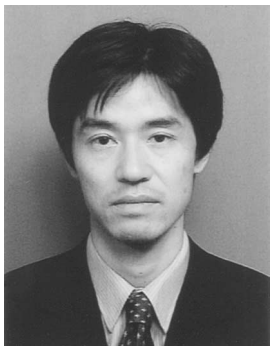

Osamu Sato was born in Sendai, Miyagi prefecture, Japan in 1964. He received his Ph.D. degree in 1994 from the University of Tokyo under the direction of Professor Akira Fujishima. He started an academic career in 1994 at the Photochemical Conversion Materials Project in the Kanagawa Academy of Science and Technology (KAST) as a researcher. In 1998, he became a director of the Special Research Laboratory for Optical Science in KAST. He was awarded the CSJ Award for Young Chemists in 1998. His research interests include the development of photo-magnets, photo-tunable photonic crystals and the design of supramolecules exhibiting photo-bistability.

Shinya Hayami was born in Kure, Hiroshima prefecture, Japan in 1968. He received his Ph.D. degree in 1997 from Kyushu University under the direction of Professor Yonezo Maeda. He started an academic career in 1998 in the Institute for Molecular Science (IMS) as an IMS fellow. In 1999, he became a researcher at the Special Research Laboratory for Optical Science in the Kanagawa Academy of Science and Technology (KAST). Since October 2000 he has been an assistant professor of Kyushu University. His research interests include the study of spin-crossover and LIESST compounds.

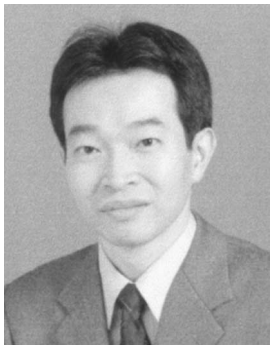

Yasuaki Einaga was born in Niigata prefecture, Japan in 1971. He received his Ph.D. degree in 1999 from the University of Tokyo under the direction of Professor Akira Fujishima. After a postdoctoral fellowship at the Special Research Laboratory for Optical Science in the Kanagawa Academy of Science and Technology (KAST), he joined Professor Fujishima's group at the University of Tokyo as a research associate (1999). In 2001, he joined the department of Chemistry at Keio University as Assistant Professor. His research interests include photo-functional materials science, Mössbauer spectroscopy and diamond as a functional material.

Zhong-Ze Gu was born in Chang Zhou, Jiangsu prefecture, China in 1968. He received his Ph.D. degree in 1998 from the University of Tokyo under the direction of Professor Akira Fujishima. He started an academic career in1998 at the Photochemical Conversion Materials Project in the Kanagawa Academy of Science and Technology (KAST) as a researcher. In the same year, he became a researcher at the Special Research Laboratory for Optical Science in KAST. His research interests include the study of molecule-based magnets, porous materials and biosensors.